iScience

CellPress

Article

The Autism-Related Protein SETD5 Controls Neural Cell Proliferation through Epigenetic Regulation of rDNA Expression

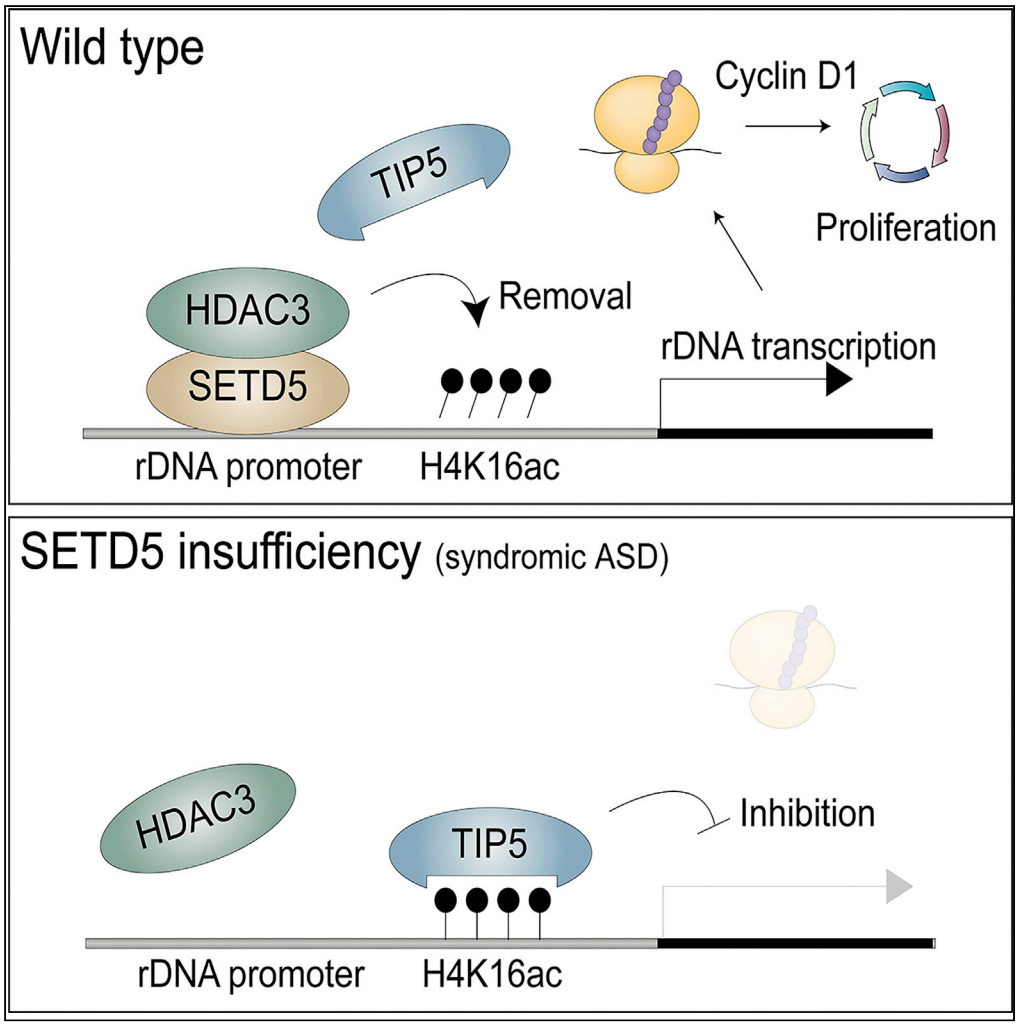

Tadashi Nakagawa, Satoko Hattori, Risa Nobuta, ..., Noriko Osumi, Keiichi I. Nakayama, Keiko Nakayama

nakayak2@med.tohoku.ac.jp

HIGHLIGHTS

Setd5$^{+/-}$ mice manifest syndromic autism-related phenotypes

SETD5 recruits the HDAC3 complex to the rDNA promoter

SETD5 deficiency reduces rRNA abundance and attenuates translational activity

SETD5 deficiency inhibits cyclin D1 mRNA translation and neural cell proliferation

Nakagawa et al., iScience *23*, 101030
April 24, 2020 © 2020 The Author(s).
https://doi.org/10.1016/j.isci.2020.101030

iScience

CellPress

Article

The Autism-Related Protein SETD5 Controls Neural Cell Proliferation through Epigenetic Regulation of rDNA Expression

Tadashi Nakagawa,[1] Satoko Hattori,[2] Risa Nobuta,[3] Ryuichi Kimura,[4] Makiko Nakagawa,[1] Masaki Matsumoto,[5] Yuko Nagasawa,[1] Ryo Funayama,[1] Tsuyoshi Miyakawa,[2] Toshifumi Inada,[3] Noriko Osumi,[4] Keiichi I. Nakayama,[5] and Keiko Nakayama[1,6,*]

SUMMARY

Haploinsufficiency of SETD5 is implicated in syndromic autism spectrum disorder (ASD), but the molecular mechanism underlying the pathological role of this protein has remained unclear. We have now shown that *Setd5*$^{+/-}$ mice manifest ASD-related behavioral phenotypes and that the expression of ribosomal protein genes and rDNA is disturbed in the brain of these mice. SETD5 recruited the HDAC3 complex to the rDNA promoter, resulting in removal of the histone mark H4K16ac and its reader protein TIP5, a repressor of rDNA expression. Depletion of SETD5 attenuated rDNA expression, translational activity, and neural cell proliferation, whereas ablation of TIP5 in SETD5-deficient cells rescued these effects. Translation of cyclin D1 mRNA was specifically down-regulated in SETD5-insufficient cells. Our results thus suggest that SETD5 positively regulates rDNA expression via an HDAC3-mediated epigenetic mechanism and that such regulation is essential for translation of cyclin D1 mRNA and neural cell proliferation.

INTRODUCTION

Autism spectrum disorder (ASD) is a neurodevelopmental disorder that affects nearly 1% of the human population and is characterized by impairment of social communication and restricted and repetitive behaviors (de la Torre-Ubieta et al., 2016). ASD has been classified into syndromic and nonsyndromic types, with patients with syndromic type manifesting additional phenotypes such as intellectual disability (ID), attention-deficit/hyperactivity disorder, epilepsy, and craniofacial dysmorphology. Although most cases of nonsyndromic ASD are thought to be polygenic in etiology (Sztainberg and Zoghbi, 2016), most cases of syndromic ASD appear to be caused by chromosomal abnormalities, submicroscopic copy number variations, or single-gene mutations, thus providing an opportunity to investigate the molecular mechanisms underlying ASD pathophysiology with the use of targeted gene modification in cellular and animal models. Indeed, ASD-related mutations have been found to impair a variety of cellular processes including neurogenesis, neurite growth, and synaptic plasticity (Gilbert and Man, 2017). Accumulating evidence indicates that three major cellular activities are commonly affected by ASD-related gene mutations: protein translation, WNT signaling, and synaptic signaling (de la Torre-Ubieta et al., 2016).

De novo heterozygous deletion of the gene for SET domain-containing 5 (SETD5) has recently been identified in patients with ID and ASD phenotypes (Fernandes et al., 2018; Green et al., 2017; Grozeva et al., 2014; Kuechler et al., 2015; Pinto et al., 2014; Powis et al., 2018; Stur et al., 2017; Szczaluba et al., 2016). SETD5 is a ubiquitously expressed protein (Osipovich et al., 2016) that belongs to the SET domain-containing protein family (Herz et al., 2013). The SET domains of most proteins catalyze protein lysine methylation, but those of SETD5 and its paralog MLL5 lack methyltransferase activity as a result of amino acid substitutions at several critical positions (Deliu et al., 2018; Madan et al., 2009; Mas et al., 2016). Instead, SETD5 was recently shown to bind to two chromatin-regulating complexes—the polymerase-associated factor 1 (PAF1) and histone deacetylase 3 (HDAC3) complexes (Deliu et al., 2018; Osipovich et al., 2016; Yu et al., 2017)—suggesting that SETD5 contributes to epigenetic regulation and control of gene expression through its association with these complexes. Importantly, heterozygous loss-of-function mutations in genes encoding several components of the HDAC3 complex have been identified in individuals with ASD or ID (O'Roak et al., 2012; Pons et al., 2015; Sirmaci et al., 2011), suggestive of a functional link between SETD5 and the HDAC3 complex in the pathogenesis of ASD and ID. However, whether or how SETD5 regulates gene expression related to ASD and ID has remained unclear.

[1]Division of Cell Proliferation, ART, Graduate School of Medicine, Tohoku University, Sendai, Miyagi 980-8575, Japan

[2]Division of Systems Medical Science, Institute for Comprehensive Medical Science, Fujita Health University, Toyoake, Aichi 470-1192, Japan

[3]Graduate School of Pharmaceutical Science, Tohoku University, Sendai, Miyagi 980-8578, Japan

[4]Division of Developmental Neuroscience, ART, Graduate School of Medicine, Tohoku University, Sendai, Miyagi 980-8575, Japan

[5]Department of Molecular and Cellular Biology, Medical Institute of Bioregulation, Kyushu University, Fukuoka 812-8582, Japan

[6]Lead Contact

*Correspondence: nakayak2@med.tohoku.ac.jp

https://doi.org/10.1016/j.isci.2020.101030

This is an open access article under the CC BY-NC-ND license (http://creativecommons.org/licenses/by-nc-nd/4.0/).

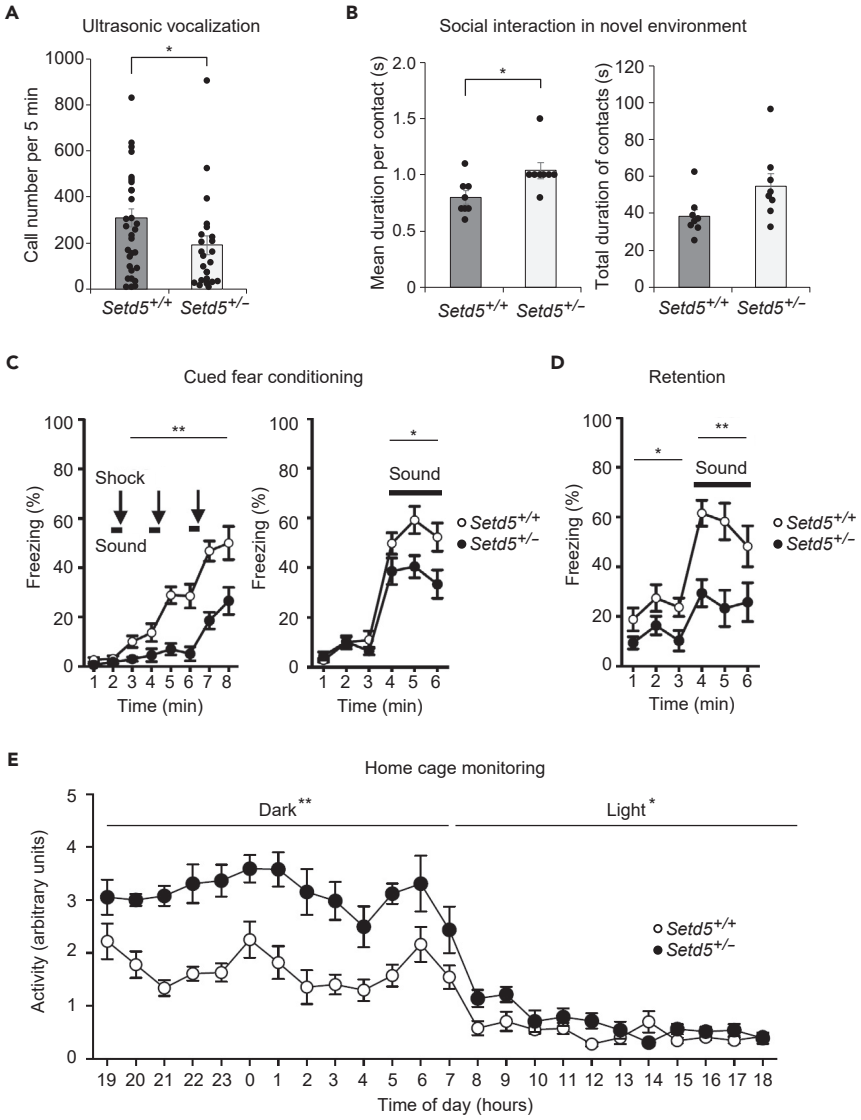

Figure 1. Behavioral Abnormalities of *Setd5*$^{+/-}$ Mice

(A) Social communication of neonatal *Setd5*$^{+/+}$ or *Setd5*$^{+/-}$ mice assessed by the ultrasonic vocalization test at postnatal day 6. Call number over 5 min was determined. Data are means ± SEM (n = 30, *Setd5*$^{+/+}$; n = 25, *Setd5*$^{+/-}$). *p < 0.05 (rank-sum test).

(B) Social interaction of adult mice assessed in a novel environment. Two mice of the same genotype and sex that had been housed in different cages were placed together in a box. Mean duration time per contact and total duration time of contacts were determined. Data are means ± SEM (n = 8 for each genotype). *p < 0.05 by one-way analysis of variance (ANOVA).

(C) Association memory formation in adult mice assessed by the cued fear-conditioning test. A conditioned stimulus of sound (55-dB white noise for 30 s) and aversive unconditioned stimulus of foot shock (0.3 mA for 2 s) were given during the indicated periods. The percentage time for freezing behavior in consecutive blocks of 1 min during the conditioning phase (left panel) and cued testing on the following day (right panel) was determined. Data are means ± SEM (n = 17 for each genotype). *p < 0.05, **p < 0.01 (two-way repeated-measures ANOVA).

(D) Association memory retention in adult mice assessed by the cued fear-conditioning test. Cued testing as in (C) was performed 1 month after the last conditioning. Data are means ± SEM (n = 17 for each genotype). *p < 0.05, **p < 0.01 (two-way repeated-measures ANOVA).

(E) Activity level of adult mice assessed by monitoring of the home cage over 24 h. Two mice of the same genotype and sex that had been housed in different cages were placed together in a box, and their activity was continuously monitored over

Figure 1. *Continued*
24 h. Data for 7 days are shown compressed and are means ± SEM (n = 8 per genotype). *p < 0.05, **p < 0.01 (two-way repeated-measures ANOVA).
See also Figures S1–S4 as well as Table S1.

We have now subjected *Setd5*$^{+/-}$ mice to comprehensive behavioral analysis and thereby shown that these animals manifest phenotypes similar to those of patients with ASD and ID. Transcriptomics analysis of the brain of *Setd5*$^{+/-}$ mice revealed impairment of the expression of rDNA as well as of ribosomal protein genes. Given that rRNA, which is encoded by rDNA, is also a key structural component of ribosomes, we analyzed the regulation of rDNA expression by SETD5 with the use of neuroblastoma cell lines. We found that SETD5 binds to the rDNA promoter and thereby recruits HDAC3, which reduces the amount of the Lys^{16}-acetylated form of histone 4 (H4K16ac) and thereby triggers the dissociation of TIP5 and promotes rDNA expression. We also found that depletion of rRNA induced by SETD5 deficiency results in attenuation of cell proliferation in cultured neuroblastoma cells, and a reduced extent of cell proliferation was also detected in the brain of *Setd5*$^{+/-}$ mouse embryos *in vivo* as well as in adult neural stem cells of these mice *in vitro*. In addition, translation of cyclin D1 mRNA was found to be specifically down-regulated in SETD5-deficient cells. Together, our findings reveal that SETD5 plays a key role in neural cell proliferation through regulation of rDNA expression at the epigenetic level.

RESULTS

Setd5$^{+/-}$ Mice Manifest Syndromic ASD Phenotypes

To examine the consequences of heterozygous deletion of *Setd5 in vivo*, we obtained *Setd5*$^{+/-}$ mice generated by the International Mouse Phenotyping Consortium (Figure S1) and determined whether these animals manifest phenotypes similar to those of humans with syndromic ASD. Consistent with a previous study (Deliu et al., 2018), *Setd5*$^{+/-}$ mice were smaller than their wild-type (WT) littermates (Figure S2A). In contrast, we did not observe any significant difference between *Setd5*$^{+/-}$ mice and WT littermates with regard to body temperature (Figure S2B), grip strength and balance in the wire-hang test (Figure S2C), or performance in the light-dark transition test (Figure S2D), the open-field test (Figure S2E), the elevated plus-maze test (Figure S2F), the Porsolt forced-swim test (Figure S2G), and the tail-suspension test (Figure S2H), revealing that *Setd5*$^{+/-}$ mice do not manifest anxiety- or depression-related behaviors.

We then performed social behavioral tests with *Setd5*$^{+/-}$ mice. In the neonatal ultrasonic vocalization test, which assesses early communicative behavior of pups toward the mother (Scattoni et al., 2009), *Setd5*$^{+/-}$ mice emitted substantially fewer ultrasonic vocalizations than did WT littermates (Figure 1A). In the social-interaction test in a novel environment, there was no difference between genotypes in the total number of contacts (47 ± 2 and 53 ± 4 events for WT and *Setd5*$^{+/-}$ mice, respectively, p = 0.271), but the mean duration per contact was significantly increased and the total duration of contacts tended to be increased (p = 0.054) in *Setd5*$^{+/-}$ mice compared with WT littermates (Figure 1B). *Setd5*$^{+/-}$ mice and WT mice performed similarly in three-chamber sociability and social preference tests (Figure S3).

To assess memory performance, we subjected mice to a cued fear-conditioning test. During the training phase, *Setd5*$^{+/-}$ mice showed reduced freezing behavior compared with WT littermates (Figure 1C), and this difference was maintained in the subsequent test phase (Figure 1D). In the Barnes maze test, *Setd5*$^{+/-}$ mice took more time to reach the target hole than did the control mice (Figures S4A and S4D). The number of errors committed in reaching the target hole as well as memory accuracy did not differ significantly between *Setd5*$^{+/-}$ and WT littermates (Figures S4B, S4C, S4E, and S4F). *Setd5*$^{+/-}$ mice also made similar numbers of correct responses as did WT littermates in the T-maze spontaneous alternation task (Figure S4G and S4H). Finally, we monitored animals for 24 h in their home cage and found that *Setd5*$^{+/-}$ mice were hyperactive in both light and dark periods compared with control mice (Figure 1E). Together, these data revealed that *Setd5*$^{+/-}$ mice manifest phenotypes similar to those of syndromic ASD (Table S1).

Impaired Expression of Ribosome-Related Genes in the *Setd5*$^{+/-}$ Mouse Brain

We performed RNA-sequencing (RNA-seq) analysis of the brain of *Setd5*$^{+/-}$ and WT mice to examine the effects of reduced abundance of SETD5 on the transcriptome. Of a total of 12,333 protein-coding genes with an FPKM (fragments per kilobase of exon model per million mapped fragments) value of >1 in the WT brain, the expression of 10 genes (*Pmch*, *Cox5b*, *Rpl30*, *Ndufs5*, *Tfap2d*, *Cox8b*, *Chrna6*, *Slc6a3*,

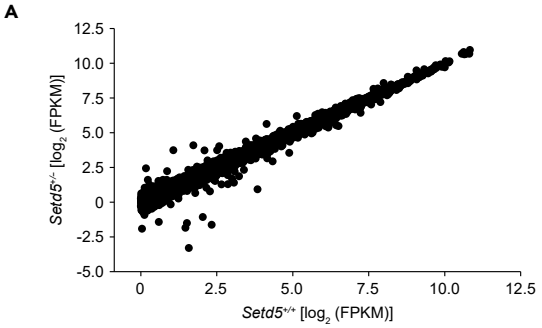

B

Down-regulated genes in *Setd5*$^{+/-}$ brain (top 5%)

Term name	p value	FDR
GO Molecular Function		
structural constituent of ribosome	2.08E-07	5.86E-05
transcriptional activator activity, RNA polymerase II proximal promoter sequence-specific DNA binding	1.40E-05	2.87E-03
ammonium ion binding	2.01E-05	3.63E-03
GO Cellular Component		
cytosolic large ribosomal subunit	1.39E-07	2.39E-05
cytosolic small ribosomal subunit	8.62E-06	9.02E-04
neuronal cell body	2.07E-05	1.95E-03

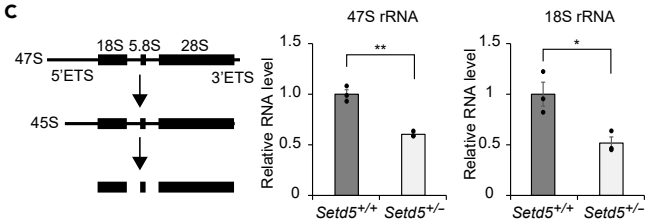

Figure 2. Impaired Ribosome-Related Gene Expression in the Brain of *Setd5*$^{+/-}$ Mice

(A) Scatterplot of gene expression levels in the brain of adult *Setd5*$^{+/+}$ and *Setd5*$^{+/-}$ mice (n = 1 for each genotype) determined by RNA-seq analysis. Only genes with an FPKM value >1 in the *Setd5*$^{+/+}$ mouse brain (12,333 genes) are shown and were subjected to GO analysis.

(B) GO analysis of molecular function and cellular component for the 617 (5%) genes showing the highest level of down-regulation in the *Setd5*$^{+/-}$ mouse brain as performed with the PANTHER overrepresentation test (Mi et al., 2013). FDR, false discovery rate.

(C) Schematic representation of rRNA maturation (ETS, external transcribed spacer) as well as RT-qPCR analysis of 47S and 18S rRNA abundance in adult mouse brain. Data are means ± SEM (n = 3 for each genotype). *p < 0.05, **p < 0.01 (Student's t test).

See also Figure S5 and Table S2.

Gm7541, *Rps8*) was found to be up-regulated, whereas that of 20 genes (*Slc6a4*, *Atp5l*, *Tph2*, *Tuba1c*, *Rpl17*, *Rpl36*, *Rps10*, *Rpl23a*, *Amd2*, *Rps29*, *Slc18a3*, *Rpl18*, *Rpl37a*, *Cyr61*, *Rln3*, *Crabp1*, *Eno1*, *Prph*, *Npas4*, *Rps7*) was down-regulated in the *Setd5*$^{+/-}$ brain with a cutoff of a 2-fold change (Figure 2A, Table S2). We then conducted Gene Ontology (GO) analysis of differentially expressed genes with the use of the PANTHER overrepresentation test (Mi et al., 2013), which revealed that genes related to transcription were enriched among those whose expression was increased in the *Setd5*$^{+/-}$ mouse brain (Figure S5A), whereas genes for ribosomal proteins were enriched among those whose expression was decreased (Figure 2B). The differences in expression of ribosomal protein genes between the two genotypes were validated by reverse transcription (RT) and quantitative polymerase chain reaction (qPCR) analysis (Figure S5B). Given that ribosomal protein expression and ribosome assembly are strongly correlated with rRNA levels (Klinge and Woolford, 2019; Xiao and Grove, 2009), we examined the abundance of rRNA, which was excluded from the RNA-seq analysis as a result of its lack of a poly(A) tail. With the use of primer sets for the primary transcript of rDNA (47S rRNA) and a processed product (18S rRNA) (Chang et al., 2009; Corsini et al., 2018), we detected a significant reduction in the amounts of both rRNA species in the *Setd5*$^{+/-}$ mouse brain compared with the WT brain (Figure 2C), implicating SETD5 in the transcription of rDNA.

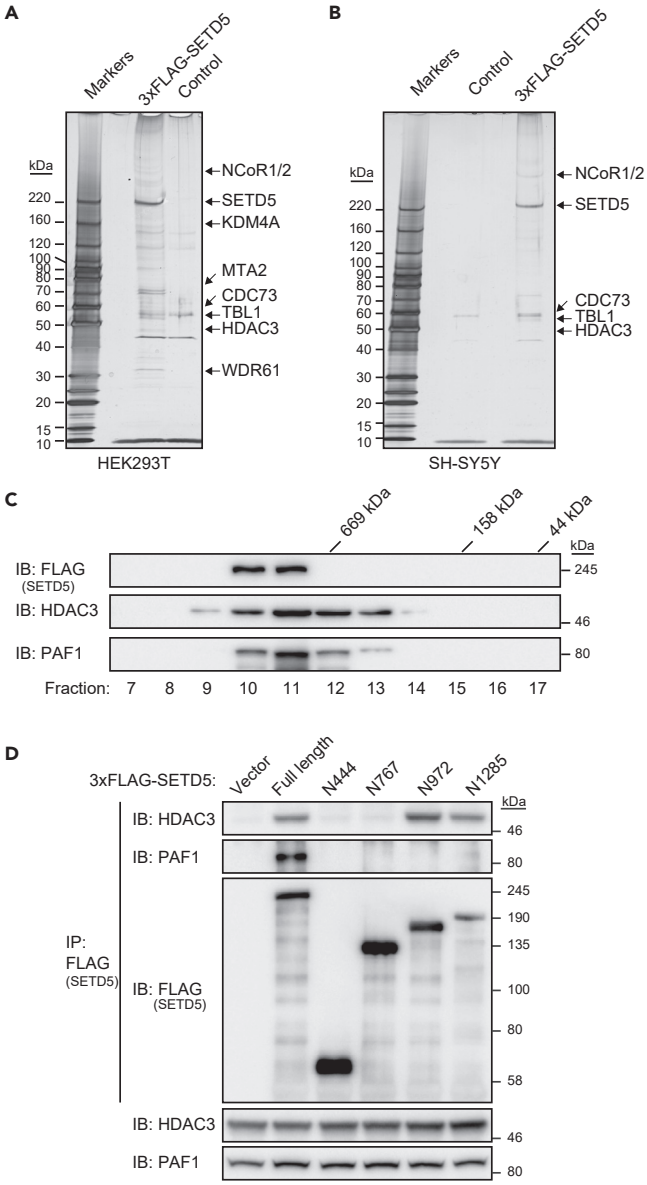

Figure 3. Association of SETD5 with HDAC3 and PAF1 Complex Components

(A) Silver staining of an SDS-PAGE gel loaded with an immunoprecipitate of 3×FLAG-tagged human SETD5 expressed in HEK293T cells. An immunoprecipitate prepared from cells transfected with the corresponding empty vector served as a control. Proteins identified by LC-MS/MS analysis are indicated.

(B) Silver staining of an SDS-PAGE gel loaded with an immunoprecipitate of 3×FLAG-SETD5 expressed in SH-SY5Y cells with the use of the doxycyline-inducible system. An immunoprecipitate prepared from corresponding cells not treated with doxycycline served as a control. Proteins identified by LC-MS/MS analysis are indicated.

(C) Immunoblot (IB) analysis of the indicated proteins in fractions obtained by gel filtration of lysates of SH-SY5Y cells expressing 3×FLAG-SETD5.

(D) Lysates of HEK293T cells expressing full-length 3×FLAG-SETD5 or the indicated deletion mutants thereof (or transfected with the corresponding empty vector) were subjected to immunoprecipitation (IP) with antibodies to FLAG, and the resulting precipitates as well as the original cell lysates were subjected to immunoblot analysis with antibodies to the indicated proteins.

See also Figure S6 and Table S3.

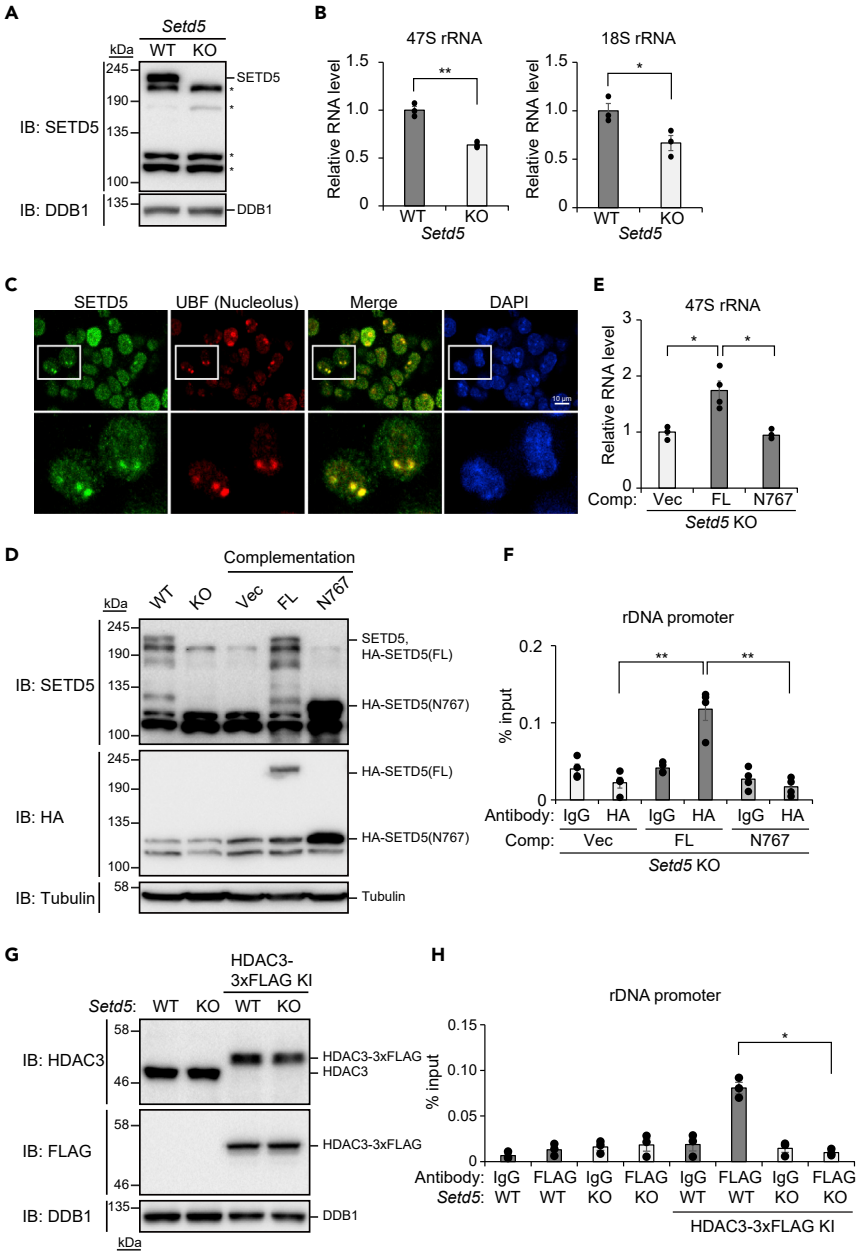

Figure 4. Recruitment of HDAC3 to the rDNA Promoter by SETD5

(A) Immunoblot analysis of SETD5 and DDB1 (loading control) in control (WT) and *Setd5* KO Neuro2a cells. Asterisks indicate nonspecific signals.

(B) RT-qPCR analysis of 47S and 18S rRNA in WT and *Setd5* KO Neuro2a cells. Data are means ± SEM (n = 3 independent experiments). *p < 0.05, **p < 0.01 (Student's t test).

(C) Immunofluorescence analysis of SETD5 and UBF (nucleolar marker) in Neuro2a cells. Nuclei were stained with 4′,6-diamidino-2-phenylindole (DAPI). The boxed regions in the upper panels are shown at higher magnification in the lower panels. Scale bar, 10 μm.

(D) Immunoblot analysis of WT or *Setd5* KO Neuro2a cells as well as of KO cells transfected with expression vectors for HA-tagged FL or N767 mutant forms of SETD5 (or with the empty vector, Vec). Tubulin served as a loading control.

(E) RT-qPCR analysis of 47S rRNA in *Setd5* KO Neuro2a cells complemented (Comp) with FL or N767 mutant forms of SETD5 as in (D). Data are means ± SEM (n = 4 independent experiments). *p < 0.05 (one-way ANOVA followed by Tukey's test).

(F) ChIP-qPCR analysis of HA-SETD5 binding to the rDNA promoter in *Setd5* KO Neuro2a cells complemented with FL or N767 forms of HA-SETD5 as in (D). ChIP was performed with antibodies to HA and with control immunoglobulin G (IgG). Data are means ± SEM (n = 4 independent experiments). **p < 0.01 (one-way ANOVA followed by Tukey's test).

Figure 4. *Continued*

(G) Immunoblot analysis of WT or *Setd5* KO Neuro2a cells as well as of WT or KO cells modified by knockin of the DNA sequence encoding the 3×FLAG tag into the *Hdac3* locus (HDAC-3×FLAG KI).

(H) ChIP-qPCR analysis of endogenous HDAC3-3×FLAG binding to the rDNA promoter in WT or *Setd5* KO Neuro2a cells engineered as in (G). ChIP was performed with antibodies to FLAG and with control IgG. Data are means ± SEM (n = 3 independent experiments). *$p < 0.05$ (one-way ANOVA followed by Tukey's test).

See also Figures S7 and S10.

SETD5 Binds to HDAC3 and PAF1 Complexes

To elucidate the molecular mechanism by which SETD5 might regulate the expression of ribosomal protein genes and rDNA, we investigated which proteins associate with SETD5. We thus expressed 3×FLAG-tagged human SETD5 in HEK293T cells, subjected cell lysates to immunoprecipitation with antibodies to FLAG, and analyzed the precipitates by liquid chromatography and tandem mass spectrometry (LC-MS/MS). Consistent with previous findings (Deliu et al., 2018; Osipovich et al., 2016; Yu et al., 2017), we detected components of the HDAC3 complex (NCoR1/2, KDM4A, MTA2, HDAC3, TBL1) and of the PAF1 complex (CDC73, WDR61) in the 3×FLAG-SETD5 immunoprecipitates (Figures 3A and S6A, and Table S3). LC-MS/MS analysis of similar immunoprecipitates prepared from SH-SY5Y cells expressing 3×FLAG-SETD5 confirmed the coprecipitation of components of the HDAC3 (NCoR1/2, TBL1, HDAC3) and PAF1 (CDC73) complexes (Figures 3B and S6B, and Table S3). Gel filtration of cell lysates prepared from SH-SY5Y cells expressing 3×FLAG-SETD5 revealed that the recombinant protein coeluted with endogenous HDAC3 and PAF1 in fractions corresponding to a molecular size of >669 kDa (Figure 3C), indicating that most 3×FLAG-SETD5 was likely present in HDAC3 and PAF1 complexes. Immunoprecipitation analysis with a series of deletion mutants of SETD5 showed that HDAC3 bound to the NH_2-terminal portion of SETD5 comprising amino acids 1 to 972, but not to one consisting of residues 1 to 767, suggesting that the region of SETD5 spanning amino acids 768 to 972 is responsible for binding to the HDAC3 complex (Figure 3D). PAF1 bound to full-length SETD5, but not to any of the deletion mutants tested, suggesting that PAF1 binds to the extreme COOH-terminal region of SETD5 (amino acids 1286–1442) (Figure 3D). Importantly, the NH_2-terminal fragments of SETD5 examined in this immunoprecipitation analysis were selected on the basis of *SETD5* mutations—including nonsense (R445X, R768X, S973X) and frameshift (S1286Lfs*84) mutations—identified in patients with ASD or ID. Patients harboring R445X or R768X nonsense mutations were reported to exhibit severe syndromic ASD phenotypes (Grozeva et al., 2014; Kuechler et al., 2015), whereas those with the S973X nonsense mutation or the S1286Lfs*84 frameshift mutation were reported to show only mild motor defects and ID without ASD or other comorbidities (Stur et al., 2017; Szczaluba et al., 2016), suggesting that loss of HDAC3 binding is critical for the pathogenesis of syndromic ASD caused by *SETD5* mutations.

Recruitment of HDAC3 to the rDNA Promoter by SETD5

We next generated Neuro2a mouse neuroblastoma cells that lack SETD5 with the use of the CRISPR/Cas9 system (Figures 4A and S7A). Consistent with data obtained with the *Setd5*$^{+/-}$ mouse brain, loss of SETD5 resulted in down-regulation of the expression of rDNA (Figure 4B). With the use of antibodies to SETD5 whose specificity was validated with the *Setd5* knockout (KO) cells (Figure S7B), we detected the apparent presence of SETD5 in the nucleolus (Figure 4C), the site of rDNA transcription (Boisvert et al., 2007). To examine whether SETD5 binds to rDNA, we engineered the *Setd5* KO cells to express hemagglutinin (HA)-epitope-tagged full-length (FL) or N767 mutant (amino acids 1–767) forms of SETD5 (Figure 4D) and then subjected the cells to chromatin immunoprecipitation (ChIP) with antibodies to HA followed by qPCR analysis with primers targeted to the rDNA gene body or its promoter region. Of note, expression of SETD5(FL) rescued the expression of rDNA in the *Setd5* KO cells (Figure 4E), excluding the possibility of an off-target effect of the KO procedure on the expression of rDNA. We detected the binding of SETD5(FL) to the rDNA promoter (Figure 4F), but not to the gene body (Figure S7C). In contrast, SETD5(N767) did not show any binding to these genomic regions (Figures 4F and S7C) and also did not restore the expression of rDNA in the *Setd5* KO cells (Figure 4E), indicating that the association of SETD5 with the rDNA promoter is mediated by the COOH-terminal portion of the protein comprising amino acids 768 to 1442 and results in the production of rRNA. To examine whether HDAC3 also binds to rDNA, we introduced the DNA sequence encoding the 3×FLAG tag into the endogenous *Hdac3* locus (HDAC3-3×FLAG KI) in both control and *Setd5* KO Neuro2a cells (Figure 4G) and performed ChIP with antibodies to FLAG followed by qPCR analysis. HDAC3 was found to bind to the rDNA promoter (Figure 4H), but not to the gene body (Figure S7D), in the control (SETD5-expressing) cells. However, this binding was not detected in the *Setd5* KO cells (Figure 4H), indicating that SETD5 recruits HDAC3 to the rDNA promoter.

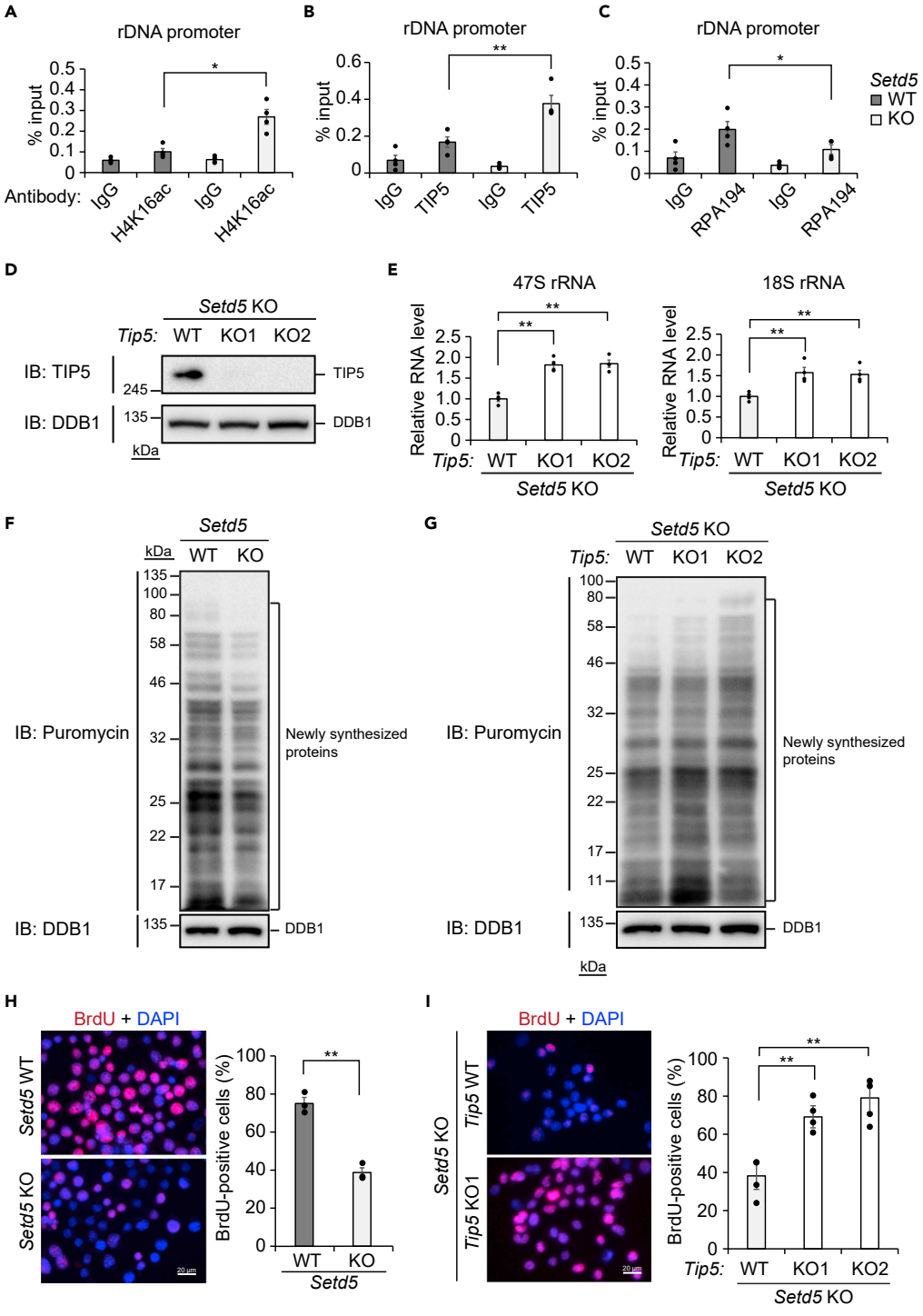

Figure 5. Essential Role of TIP5 in Repression of rDNA in *Setd5* KO Neuro2a Cells

(A–C) ChIP-qPCR analysis of H4K16ac (A), TIP5 (B), or RPA194 (C) at the rDNA promoter in WT or *Setd5* KO Neuro2a cells. Data are means ± SEM (n = 4 independent experiments). *p < 0.05, **p < 0.01 (one-way ANOVA followed by Tukey's test).

(D) Immunoblot analysis of TIP5 in *Setd5* KO Neuro2a cells with (KO1 and KO2) or without (WT) additional KO of TIP5.

(E) RT-qPCR analysis of 47S and 18S rRNA in *Setd5* KO Neuro2a cells with or without TIP5 KO. Data are means ± SEM (n = 4 independent experiments). **p < 0.01 (one-way ANOVA followed by Tukey's test).

(F and G) Immunoblot analysis of translational activity on the basis of puromycin incorporation into newly synthesized proteins in WT or *Setd5* KO Neuro2a cells (F) or in *Setd5* KO Neuro2a cells with or without TIP5 KO (G).

Figure 5. *Continued*

(H and I) Immunofluorescence analysis (left) of bromodeoxyuridine (BrdU) incorporation in WT or *Setd5* KO Neuro2a cells (H) or in *Setd5* KO Neuro2a cells with or without TIP5 KO (I). Nuclei were stained with DAPI. Scale bars, 20 μm. The percentage of BrdU-positive cells was also determined for each condition (right). Data are means ± SEM (n = 3 independent experiments). **p < 0.01 by Student's t test (H) or one-way ANOVA followed by Tukey's test (I).
See also Figures S8–S10.

TIP5 Mediates Repression of rDNA in *Setd5* KO Cells

ChIP-qPCR analysis revealed that the level of the HDAC3 substrate H4K16ac (Johnson et al., 2002) at the rDNA promoter, but not that at the gene body, was increased in *Setd5* KO cells compared with control cells (Figures 5A and S8A). TTF-I-interacting protein 5 (TIP5) was previously shown to recognize H4K16ac and thereby to recruit transcriptional repressor proteins to silence rDNA (Sharifi and Bierhoff, 2018). Consistent with these previous findings, we found that the amount of TIP5 bound to the rDNA promoter was also increased in the *Setd5* KO cells (Figure 5B). The amount of TIP5 bound to the 5′ external transcribed spacer of rDNA, but not that bound at downstream regions, was also increased in the KO cells (Figure S8B); this increase might be mediated by a mechanism independent of H4K16ac, possibly involving transcription termination factor-I (TTF-I) and long non-coding RNA (Sharifi and Bierhoff, 2018). Transcription of rDNA is silenced by the TIP5-containing nucleolar remodeling complex by establishment of heterochromatin-like features—including DNA methylation, hypoacetylation of histone 4 (mediated by HDAC1), and methylation (me) of H3K9—at the rDNA promoter (Santoro et al., 2002; Zhou et al., 2002). Consistent with these previous findings, we detected increased levels of DNA methylation (Figure S8C) and H3K9me3 (Figure S8D) at the rDNA promoter in the SETD5-deficient cells. In contrast, we found that the level of pan-acetylated histone 4 (K5+K8+K12) was increased, as was that of H4K16ac, whereas the level of pan-acetylated histone 3 (K9+K14 + K18 + K23 + K27) was reduced, in *Setd5* KO cells (Figure S8E). We speculate that TIP5 bound to H4K16ac in the *Setd5* KO cells might interfere with deacetylation of histone 4, but not with that of histone 3, or that deacetylation of histone 4 is specifically catalyzed by HDAC3 recruited by SETD5 rather than by HDAC1 bound to TIP5. SETD5 was recently found to possess intrinsic histone methyltransferase activity for H3K36 (Sessa et al., 2019). However, we did not detect a reduction in the level of H3K36me3 at the rDNA promoter in *Setd5* KO cells (Figure S8D). Given that KDM4A, which we found to be associated with SETD5 (Figure 3A), possesses H3K36 demethylase activity (Whetstine et al., 2006), it is possible that loss of SETD5 results in the simultaneous loss of KDM4A from the rDNA promoter and the consequent inability to remove associated H3K36me3.

To examine further the molecular mechanism of rDNA repression in *Setd5* KO cells, we performed ChIP-qPCR analysis with antibodies to RPA194 to measure the binding of RNA polymerase I (Pol I). The amount of Pol I binding throughout the promoter and gene body of rDNA was reduced in the absence of SETD5 (Figures 5C and S8F), suggesting that SETD5 regulates rDNA transcription by promoting the recruitment of Pol I, rather than by an effect on Pol I translocation at the rDNA promoter.

To validate the role of TIP5 in repression of rDNA in *Setd5* KO cells, we knocked out *Tip5* (also known as *Baz2a*) in *Setd5* KO Neuro2a cells with the use of the CRISPR/Cas9 system (Figures 5D and S9A). Such KO of TIP5 restored the expression of rDNA in the *Setd5* KO cells (Figure 5E).

The reduction in the amount of rRNA we found to be associated with SETD5 deficiency might have been expected to impair translational activity. Consistent with this notion, we found that the extent of puromycin incorporation into newly synthesized peptides, a measure of translational activity (Schmidt et al., 2009), was reduced in *Setd5* KO cells (Figures 5F and S9B) and that this effect was reversed by ablation of TIP5 (Figures 5G and S9C). In addition, the proliferation rate of *Setd5* KO cells was reduced compared with that of WT cells (Figure 5H), and again this effect was reversed by TIP5 KO (Figure 5I). Of note, *Tip5* KO cells on the WT background (Figures S9D and S9E) did not exhibit any increase in rDNA expression (Figure S9F) or in cell proliferation (Figure S9G), indicating that repression of rDNA expression by TIP5 is minimal in WT cells. Together, these results revealed that SETD5 recruits HDAC3 to the rDNA promoter and thereby reduces the levels of H4K16ac and its reader TIP5, resulting in up-regulation of rRNA abundance, translational activity, and cell proliferation, in Neuro2a cells.

Depletion of SETD5 Impairs rDNA Expression, Translational Activity, and Cell Proliferation in SH-SY5Y Cells

To confirm that the observed effects of SETD5 loss were not restricted to mouse cells, we depleted SH-SY5Y human neuroblastoma cells of SETD5 by RNA interference (Figure S10A). The expression of rDNA

(Figure S10B), translational activity (Figure S10C), and cell proliferation (Figure S10D) were all attenuated in SH-SY5Y cells depleted of SETD5.

SETD5 Haploinsufficiency Impairs Proliferation of Neural Stem/Progenitor Cells

We next investigated the effect of SETD5 haploinsufficiency on neural cell proliferation *in vivo*. Immunoblot analysis revealed that the abundance of SETD5 was markedly greater in the embryonic mouse brain than in the neonatal brain (Figure 6A). Immunofluorescence staining of the brain at embryonic day (E) 15 showed the presence of SETD5 in the nucleus of SOX2-positive neural stem/progenitor cells as well as in that of more differentiated cells located outside of the ventricular zone (Figure 6B), indicating that the expression of SETD5 begins early in the differentiation process of neural stem/progenitor cells and continues in differentiated neuronal cells. Immunostaining of the E15 brain with antibodies to Ki67, a marker of cell proliferation, revealed that the proportion of Ki67-positive cells was reduced in *Setd5*$^{+/-}$ mice compared with WT littermates (Figure 6C), indicative of impairment of cell proliferation by SETD5 haploinsufficiency. To determine whether SETD5 also regulates proliferation of adult neural stem cells, we performed a neurosphere formation assay with cells derived from the adult *Setd5*$^{+/-}$ mouse brain. The brain of *Setd5*$^{+/-}$ mice contained fewer neurosphere-initiating cells than did the WT brain (Figure 6D). Furthermore, the extent of rDNA expression was significantly reduced in neurospheres formed by *Setd5*$^{+/-}$ cells compared with those formed by WT cells (Figure 6E). Together, these results thus indicated that SETD5 positively regulates the proliferation of neural stem/progenitor cells in both the embryonic and adult mouse brain.

Translation of Cyclin D1 mRNA Is Down-regulated in *Setd5* KO Cells

Finally, we explored the molecular mechanism by which SETD5 haploinsufficiency impairs cell proliferation. Analysis of cell cycle profile by flow cytometric analysis after staining with 5-bromo-2′-deoxyuridine and propidium iodide showed that the proportion of cells in G_1 phase was increased and that in S phase was reduced for *Setd5* KO cells compared with WT cells, indicative of G_1 arrest in the former cells (Figure 7A). Given that expression of G_1-S cyclins is required for G_1 to S progression (Liu et al., 2019), we examined the translation of mRNAs encoding such proteins that have been shown to be subject to translational regulation: cyclin D1, cyclin E1, and cyclin E2 (Tarn and Lai, 2011). RT-qPCR analysis of mRNAs associated with polysome and monosome fractions revealed a shift of cyclin D1 mRNA, but not of cyclin E1 and cyclin E2 mRNAs, from polysomes to monosomes in *Setd5* KO cells compared with WT cells, suggesting that translation of cyclin D1 mRNA is specifically down-regulated as a result of SETD5 deficiency (Figures 7B–7F). Consistent with these findings, the amount of cyclin D1 protein, but not that of the corresponding mRNA, was reduced, whereas those of cyclin E1 and cyclin E2 proteins and mRNAs were not affected, in *Setd5* KO cells (Figures 7G and 7H). We also detected a reduction in the amount of cyclin D1 protein in the E15.5 brain of *Setd5*$^{+/-}$ mice compared with that of WT mice (Figure 7I). Together, these results indicated that SETD5 insufficiency attenuates the translation of cyclin D1 mRNA and thereby restrains cell proliferation. Given that cyclin D1 KO mice manifest neurological phenotypes (Sicinski et al., 1995) and that cyclin D1 is implicated in ASD-related protein-protein interaction networks (Neale et al., 2012), we hypothesize that down-regulation of cyclin D1 and the consequent impairment of neural cell proliferation are responsible at least in part for the ASD-like phenotypes of *Setd5*$^{+/-}$ mice.

DISCUSSION

Translation is one of the three major cellular activities shown to be disrupted in patients with ASD (de la Torre-Ubieta et al., 2016). However, whether or how rDNA expression, which is required for ribosome production, is related to syndromic ASD has been unexplored. We have now shown that SETD5 regulates the expression of rDNA at the epigenetic level and that SETD5 haploinsufficiency gives rise to syndromic-ASD-like phenotypes in mice. SETD5 was found to recruit the HDAC3 complex to the rDNA promoter, resulting in the removal of both H4K16ac and its reader TIP5 and a consequent increase in rDNA transcription by Pol I. A reduction in the amount of SETD5 thus resulted in attenuation of rRNA production, translational activity, and cell proliferation.

During the preparation of our manuscript, several studies of *Setd5*$^{+/-}$ mice, including behavioral analyses, were published (Deliu et al., 2018; Moore et al., 2019; Sessa et al., 2019). Our results are mostly consistent with those of these previous studies showing ASD-related behavioral phenotypes of the mutant mice

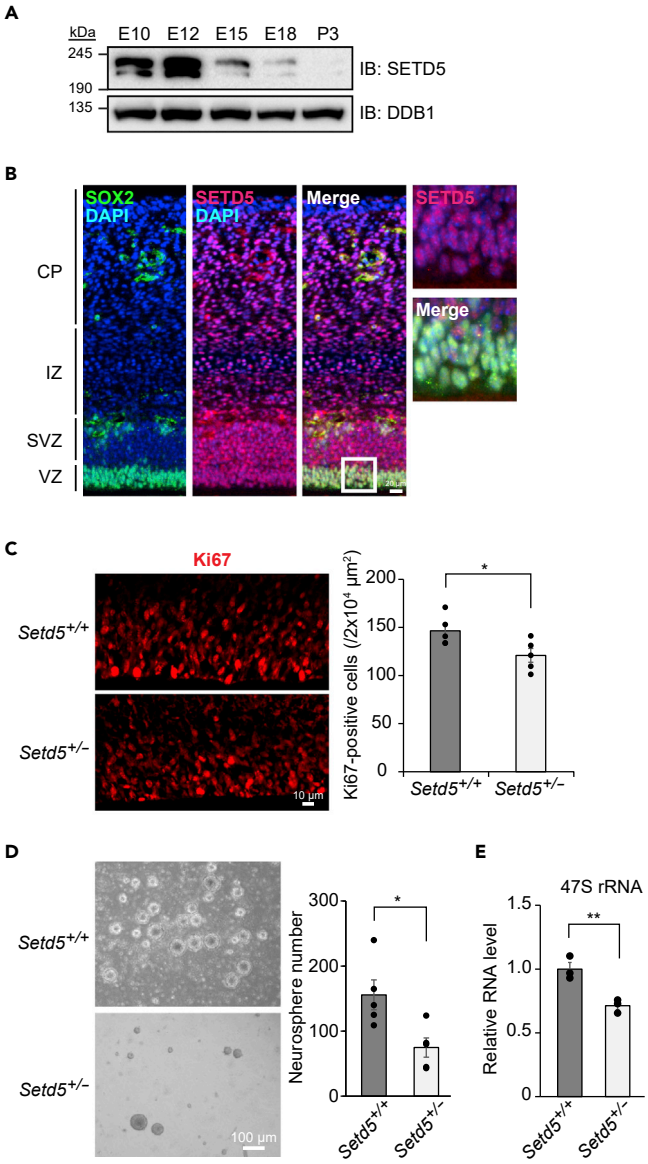

Figure 6. Impaired Proliferation of Neural Stem/Progenitor Cells in the Embryonic and Adult Brain of *Setd5*$^{+/-}$ Mice

(A) Immunoblot analysis of SETD5 in mouse brain from embryonic day (E) 10 to postnatal day (P) 3.

(B) Immunohistofluorescence staining of SOX2 and SETD5 in a cortical section of the E15 mouse brain. Nuclei were stained with DAPI. The boxed region in the merged image is shown at higher magnification on the right. Scale bar, 20 μm. CP, cortical plate; IZ, intermediate zone; SVZ, subventricular zone; VZ, ventricular zone.

(C) Immuohistofluorescence staining of Ki67 in the ventricular zone of the *Setd5*$^{+/+}$ or *Setd5*$^{+/-}$ mouse brain at E15. Scale bar, 10 μm. The numbers of Ki67-positive cells were determined as mean ± SEM values (n = 5 for each genotype). *p < 0.05 (Student's t test).

(D) Phase-contrast microscopic images of neurospheres derived from the brain of adult *Setd5*$^{+/+}$ or *Setd5*$^{+/-}$ mice. Scale bar, 100 μm. The numbers of neurospheres were also determined as means ± SEM (n = 5 for each genotype). *p < 0.05 (Student's t test).

(E) RT-qPCR analysis of 47S rRNA in neurospheres derived from the brain of adult *Setd5*$^{+/+}$ or *Setd5*$^{+/-}$ mice. Data are means ± SEM (n = 3 for each genotype). **p < 0.01 (Student's t test).

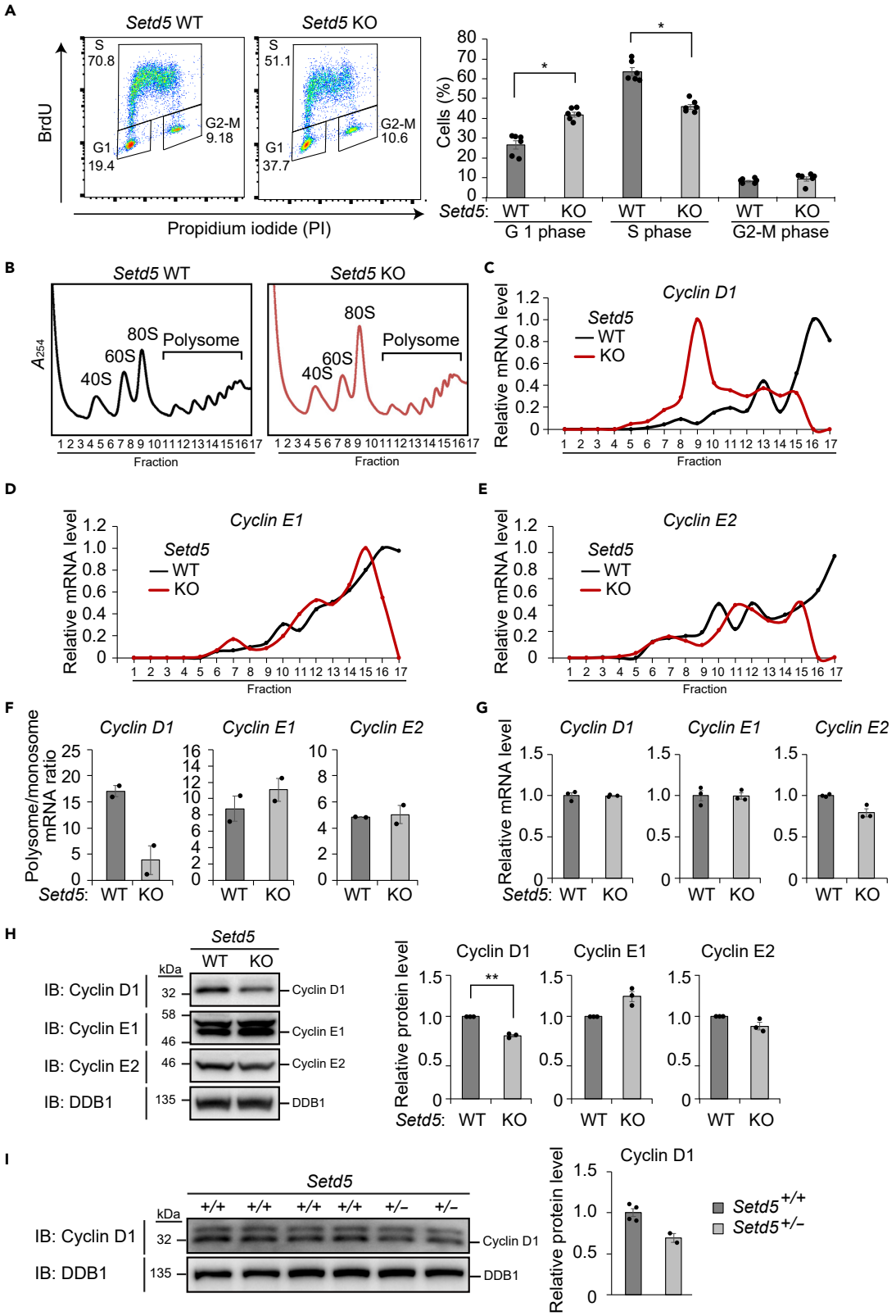
A
Setd5 WT
Setd5 KO
BrdU
Propidium iodide (PI)
S 70.8
G1 19.4
G2-M 9.18
S 51.1
G1 37.7
G2-M 10.6
Cells (%)
Setd5: WT KO WT KO WT KO
G 1 phase
S phase
G2-M phase
B
Setd5 WT
Setd5 KO
A254
40S
60S
80S
Polysome
Fraction
C
Cyclin D1
Setd5
WT
KO
Relative mRNA level
Fraction
D
Cyclin E1
E
Cyclin E2
F
Cyclin D1
Cyclin E1
Cyclin E2
Polysome/monosome mRNA ratio
G
H
Setd5
kDa
IB: Cyclin D1
IB: Cyclin E1
IB: Cyclin E2
IB: DDB1
Relative protein level
I
+/+ +/+ +/+ +/+ +/− +/−
Setd5+/+
Setd5+/−

Figure 7. Down-regulation of Cyclin D1 mRNA Translation in *Setd5* KO Neuro2a Cells

(A) Flow cytometric analysis of the cell cycle in WT and *Setd5* KO Neuro2a cells stained with bromodeoxyuridine (BrdU) and propidium iodide (PI). Representative profiles as well as mean ± SEM values for the proportion of cells in each phase of the cell cycle (n = 6 independent experiments) are shown. *$p < 0.05$ (Student's t test).

(B) Ribosome fractionation by sucrose gradient centrifugation for WT and *Setd5* KO Neuro2a cells as revealed by measurement of absorbance at 254 nm (A_{254}). Fractions 9 and 10 were assayed as 80S monosomes, and fractions 11 to 17, as polysomes.

(C–E) Representative RT-qPCR analysis of mRNAs for cyclin D1 (C), cyclin E1 (D), and cyclin E2 (E) in ribosome fractions of WT and *Setd5* KO Neuro2a cells.

(F) The polysome/monosome ratio for cyclin D1, cyclin E1, and cyclin E2 mRNAs determined as in (C–E). Data are means ± SEM (n = 2 independent experiments).

(G) RT-qPCR analysis of mRNAs for cyclin D1, cyclin E1, and cyclin E2 in WT and *Setd5* KO Neuro2a cells. Data are means ± SEM (n = 3 independent experiments).

(H) Immunoblot analysis of cyclin D1, cyclin E1, and cyclin E2 in WT and *Setd5* KO Neuro2a cells. DDB1 served as a loading control. Representative blots as well as quantitative data presented as means ± SEM (n = 3 independent experiments) are shown. **$p < 0.01$ (Student's t test).

(I) Immunoblot analysis of cyclin D1 in the E15.5 brain of $Setd5^{+/+}$ and $Setd5^{+/-}$ mice. Representative blots as well as quantitative data presented as means ± SEM (n = 4, $Setd5^{+/+}$; n = 2, $Setd5^{+/-}$) are shown.

including impaired social behavior and cognitive function as well as increased locomotor activity (Table S1), although we did not detect increased anxiety-like behavior in the elevated plus-maze test (Figure S2F). Our results on the effect of SETD5 deficiency on cell proliferation also differ from those reported in these previous studies (Deliu et al., 2018; Moore et al., 2019; Sessa et al., 2019). These apparent discrepancies might be due to differences in genetic background of the mice studied, in the methods adopted for disruption of *Setd5*, in animal housing conditions, in the age of embryos examined, or in the methods applied for measurement of cell proliferation. Further analyses are required to elucidate the reasons for the discrepant findings.

In general, HDACs are thought to function as repressors of transcription (Seto and Yoshida, 2014). In the case of rDNA, HDAC1 has been shown to down-regulate its expression (Sharifi and Bierhoff, 2018). In contrast, our data now indicate that HDAC3—a member of the class I HDAC family that includes HDAC1, HDAC2, and HDAC8—up-regulates rDNA expression. Of note, HDAC3 was previously shown to activate transcription controlled by retinoic acid–responsive elements (Jepsen et al., 2000). In addition, cells derived from HDAC3 KO mice manifest not only up-regulation but also down-regulation of gene expression (Bhaskara et al., 2008). These observations suggest that transcriptional activation by HDAC3 is not limited to rDNA. It will be of interest to determine the genomic contexts in which HDAC3 functions as either a transcriptional activator or a transcriptional repressor. In this regard, histone deacetylation at the rDNA promoter in cells might provide a model system to identify relevant histone substrates of HDAC3 and other class I HDAC family members, given that the attempted identification of such substrates with purified proteins has yielded conflicting and inconsistent results *in vitro* (Seto and Yoshida, 2014). Of particular interest is our finding that the level of histone 3 acetylation is decreased, whereas that of histone 4 acetylation is increased in SETD5-deficient Neuro2a cells (Figure S8E).

We focused on impaired cell proliferation as a cellular phenotype induced by deficiency of SETD5, given that this phenotype was readily detectable by microscopy during cell culture. Knockdown of SETD5 was recently shown to attenuate the proliferation of a human prostate carcinoma cell line (Zhang et al., 2019), indicating that regulation of cell proliferation by SETD5 might not be specific to neural cells. Our polysome analysis revealed that the translation of cyclin D1 mRNA was down-regulated in SETD5-insufficient cells. It remains unclear how the translation of cyclin D1 mRNA, but not that of cyclin E1 and cyclin E2 mRNAs, is sensitive to the loss of SETD5. Given that mechanistic target of rapamycin complex 1 (mTORC1) (Frost et al., 2009; Holmes et al., 2016) and heterogeneous nuclear ribonucleoprotein A1 (hnRNPA1) (Gao et al., 2017) are both implicated in the regulation of cyclin D1 mRNA translation, it is likely that several mechanisms, which might be regulated by SETD5 independently of translation, may play a role in this selectivity. The findings that cyclin D1 KO mice manifest neurological phenotypes (Sicinski et al., 1995) and that cyclin D1 is implicated in ASD-related protein-protein interaction networks (Neale et al., 2012) suggest the possibility that down-regulation of cyclin D1 and the consequent disruption of neural cell proliferation are at least partially responsible for the ASD phenotypes of $Setd5^{+/-}$ mice.

In addition to cell proliferation, however, SETD5-mediated regulation of translation might be linked to other processes with relevance to ASD, such as synaptic function. In support of this notion, neurons in the brain of $Setd5^{+/-}$ mice were recently found to manifest abnormal synaptic activity (Deliu et al., 2018)

and connectivity (Moore et al., 2019). It will be of particular interest to determine the extent to which synaptic dysfunction in *Setd5*$^{+/-}$ mice is due to impairment of translation.

We found that TIP5 ablation rescued rDNA expression, translational activity, and cell proliferation in *Setd5* KO cells. These data suggest the possibility that either a drug that interferes with the binding of TIP5 to H4K16ac at the rDNA promoter or depletion of TIP5 might ameliorate phenotypes associated with SETD5 haploinsufficiency.

Limitations of the Study

Results of this study utilizing cultured neuronal cells might not exactly reflect the *in vivo* functions of neurons.

METHODS

All methods can be found in the accompanying Transparent Methods supplemental file.

SUPPLEMENTAL INFORMATION

Supplemental Information can be found online at https://doi.org/10.1016/j.isci.2020.101030.

ACKNOWLEDGMENTS

We thank the Wellcome Trust Sanger Institute Mouse Genetics Project (Sanger MGP) and its funders for providing the mutant mouse line (allele: *Setd5*$^{tm1a(EUCOMM)Wtsi}$). Funding and associated primary phenotypic information may be found at www.sanger.ac.uk/mouseportal. We thank T. Kitamura for pMX-puro and Plat-E cells, T. Sato and laboratory members for discussion, and the Biomedical Research Core of Tohoku University Graduate School of Medicine for technical support. This work was funded by Japan Society for the Promotion of Science (JSPS) KAKENHI grants 15K18365, 17K14955, and 19K07837 (to T.N.) and 17H04035 and JP16H06276 (to K.N.); a Grant-in-Aid for Scientific Research on Innovative Areas–Platform for Advanced Technologies and Research Resources (16H06276 to T.M.); and in part by the Joint Usage/Research Center for Genes, Brain, and Behavior supported by the Ministry of Education, Culture, Sports, Science and Technology of Japan.

AUTHOR CONTRIBUTIONS

T.N. designed and performed most of the experiments and cowrote the manuscript. K.N. directed and coordinated the study, oversaw the results, and cowrote the manuscript. M.N. and Y.N. assisted with experiments. S.H. coordinated and assisted with most of the mouse behavioral analyses. R.N. performed polysome analysis. R.K. performed ultrasonic vocalization tests. M.M. performed LC-MS/MS analysis. R.F. performed transcriptomics analysis. T.I., T.M., N.O., and K.I.N. provided advice. All authors discussed the results and commented on the manuscript.

DECLARATION OF INTERESTS

The authors declare no competing interests.

Received: November 1, 2019
Revised: February 29, 2020
Accepted: March 30, 2020
Published: April 24, 2020

REFERENCES

Bhaskara, S., Chyla, B.J., Amann, J.M., Knutson, S.K., Cortez, D., Sun, Z.W., and Hiebert, S.W. (2008). Deletion of histone deacetylase 3 reveals critical roles in S phase progression and DNA damage control. Mol. Cell *30*, 61–72.

Boisvert, F.M., van Koningsbruggen, S., Navascues, J., and Lamond, A.I. (2007). The multifunctional nucleolus. Nat. Rev. Mol. Cell Biol. *8*, 574–585.

Chang, T.C., Zeitels, L.R., Hwang, H.W., Chivukula, R.R., Wentzel, E.A., Dews, M., Jung, J., Gao, P., Dang, C.V., Beer, M.A., et al. (2009). Lin-28B transactivation is necessary for Myc-mediated let-7 repression and proliferation. Proc. Natl. Acad. Sci. U S A *106*, 3384–3389.

Corsini, N.S., Peer, A.M., Moeseneder, P., Roiuk, M., Burkard, T.R., Theussl, H.C., Moll, I., and Knoblich, J.A. (2018). Coordinated control of mRNA and rRNA processing controls embryonic stem cell pluripotency and differentiation. Cell Stem Cell *22*, 543–558.e12.

de la Torre-Ubieta, L., Won, H., Stein, J.L., and Geschwind, D.H. (2016). Advancing the understanding of autism disease mechanisms through genetics. Nat. Med. *22*, 345–361.

Deliu, E., Arecco, N., Morandell, J., Dotter, C.P., Contreras, X., Girardot, C., Kasper, E.L., Kozlova, A., Kishi, K., Chiaradia, I., et al. (2018). Haploinsufficiency of the intellectual disability gene SETD5 disturbs developmental gene expression and cognition. Nat. Neurosci. *21*, 1717–1727.

Fernandes, I.R., Cruz, A.C.P., Ferrasa, A., Phan, D., Herai, R.H., and Muotri, A.R. (2018). Genetic variations on SETD5 underlying autistic conditions. Dev. Neurobiol. *78*, 500–518.

Frost, P., Shi, Y., Hoang, B., Gera, J., and Lichtenstein, A. (2009). Regulation of D-cyclin translation inhibition in myeloma cells treated with mammalian target of rapamycin inhibitors: rationale for combined treatment with extracellular signal-regulated kinase inhibitors and rapamycin. Mol. Cancer Res. *8*, 83–93.

Gao, G., Dhar, S., and Bedford, M.T. (2017). PRMT5 regulates IRES-dependent translation via methylation of hnRNP A1. Nucleic Acids Res. *45*, 4359–4369.

Gilbert, J., and Man, H.Y. (2017). Fundamental elements in autism: from neurogenesis and neurite growth to synaptic plasticity. Front. Cell. Neurosci. *11*, 359.

Green, C., Willoughby, J., Study, D.D.D., and Balasubramanian, M. (2017). De novo SETD5 loss-of-function variant as a cause for intellectual disability in a 10-year old boy with an aberrant blind ending bronchus. Am. J. Med. Genet. A *173*, 3165–3171.

Grozeva, D., Carss, K., Spasic-Boskovic, O., Parker, M.J., Archer, H., Firth, H.V., Park, S.M., Canham, N., Holder, S.E., Wilson, M., et al. (2014). De novo loss-of-function mutations in SETD5, encoding a methyltransferase in a 3p25 microdeletion syndrome critical region, cause intellectual disability. Am. J. Hum. Genet. *94*, 618–624.

Herz, H.M., Garruss, A., and Shilatifard, A. (2013). SET for life: biochemical activities and biological functions of SET domain-containing proteins. Trends Biochem. Sci. *38*, 621–639.

Holmes, B., Lee, J., Landon, K.A., Benavides-Serrato, A., Bashir, T., Jung, M.E., Lichtenstein, A., and Gera, J. (2016). Mechanistic target of rapamycin (mTOR) inhibition synergizes with reduced internal ribosome entry site (IRES)-mediated translation of cyclin D1 and c-MYC mRNAs to treat glioblastoma. J. Biol. Chem. *291*, 14146–14159.

Jepsen, K., Hermanson, O., Onami, T.M., Gleiberman, A.S., Lunyak, V., McEvilly, R.J., Kurokawa, R., Kumar, V., Liu, F., Seto, E., et al. (2000). Combinatorial roles of the nuclear receptor corepressor in transcription and development. Cell *102*, 753–763.

Johnson, C.A., White, D.A., Lavender, J.S., O'Neill, L.P., and Turner, B.M. (2002). Human class I histone deacetylase complexes show enhanced catalytic activity in the presence of ATP and co-immunoprecipitate with the ATP-dependent chaperone protein Hsp70. J. Biol. Chem. *277*, 9590–9597.

Klinge, S., and Woolford, J.L., Jr. (2019). Ribosome assembly coming into focus. Nat. Rev. Mol. Cell Biol. *20*, 116–131.

Kuechler, A., Zink, A.M., Wieland, T., Ludecke, H.J., Cremer, K., Salviati, L., Magini, P., Najafi, K., Zweier, C., Czeschik, J.C., et al. (2015). Loss-of-function variants of SETD5 cause intellectual disability and the core phenotype of microdeletion 3p25.3 syndrome. Eur. J. Hum. Genet. *23*, 753–760.

Liu, L., Michowski, W., Kolodziejczyk, A., and Sicinski, P. (2019). The cell cycle in stem cell proliferation, pluripotency and differentiation. Nat. Cell Biol. *21*, 1060–1067.

Madan, V., Madan, B., Brykczynska, U., Zilbermann, F., Hogeveen, K., Dohner, K., Dohner, H., Weber, O., Blum, C., Rodewald, H.R., et al. (2009). Impaired function of primitive hematopoietic cells in mice lacking the Mixed-Lineage-Leukemia homolog MLL5. Blood *113*, 1444–1454.

Mas, Y.M.S., Barbon, M., Teyssier, C., Demene, H., Carvalho, J.E., Bird, L.E., Lebedev, A., Fattori, J., Schubert, M., Dumas, C., et al. (2016). The human mixed lineage leukemia 5 (MLL5), a sequentially and structurally divergent SET domain-containing protein with no intrinsic catalytic activity. PLoS One *11*, e0165139.

Mi, H., Muruganujan, A., and Thomas, P.D. (2013). PANTHER in 2013: modeling the evolution of gene function, and other gene attributes, in the context of phylogenetic trees. Nucleic Acids Res. *41*, D377–D386.

Moore, S.M., Seidman, J.S., Ellegood, J., Gao, R., Savchenko, A., Troutman, T.D., Abe, Y., Stender, J., Lee, D., Wang, S., et al. (2019). Setd5 haploinsufficiency alters neuronal network connectivity and leads to autistic-like behaviors in mice. Transl. Psychiatry *9*, 24.

Neale, B.M., Kou, Y., Liu, L., Ma'ayan, A., Samocha, K.E., Sabo, A., Lin, C.F., Stevens, C., Wang, L.S., Makarov, V., et al. (2012). Patterns and rates of exonic de novo mutations in autism spectrum disorders. Nature *485*, 242–245.

O'Roak, B.J., Vives, L., Fu, W., Egertson, J.D., Stanaway, I.B., Phelps, I.G., Carvill, G., Kumar, A., Lee, C., Ankenman, K., et al. (2012). Multiplex targeted sequencing identifies recurrently mutated genes in autism spectrum disorders. Science *338*, 1619–1622.

Osipovich, A.B., Gangula, R., Vianna, P.G., and Magnuson, M.A. (2016). Setd5 is essential for mammalian development and the co-transcriptional regulation of histone acetylation. Development *143*, 4595–4607.

Pinto, D., Delaby, E., Merico, D., Barbosa, M., Merikangas, A., Klei, L., Thiruvahindrapuram, B., Xu, X., Ziman, R., Wang, Z., et al. (2014). Convergence of genes and cellular pathways dysregulated in autism spectrum disorders. Am. J. Hum. Genet. *94*, 677–694.

Pons, L., Cordier, M.P., Labalme, A., Till, M., Louvrier, C., Schluth-Bolard, C., Lesca, G., Edery, P., and Sanlaville, D. (2015). A new syndrome of intellectual disability with dysmorphism due to TBL1XR1 deletion. Am. J. Med. Genet. A *167A*, 164–168.

Powis, Z., Farwell Hagman, K.D., Mroske, C., McWalter, K., Cohen, J.S., Colombo, R., Serretti, A., Fatemi, A., David, K.L., Reynolds, J., et al. (2018). Expansion and further delineation of the SETD5 phenotype leading to global developmental delay, variable dysmorphic features, and reduced penetrance. Clin. Genet. *93*, 752–761.

Santoro, R., Li, J., and Grummt, I. (2002). The nucleolar remodeling complex NoRC mediates heterochromatin formation and silencing of ribosomal gene transcription. Nat. Genet. *32*, 393–396.

Scattoni, M.L., Crawley, J., and Ricceri, L. (2009). Ultrasonic vocalizations: a tool for behavioural phenotyping of mouse models of neurodevelopmental disorders. Neurosci. Biobehav. Rev. *33*, 508–515.

Schmidt, E.K., Clavarino, G., Ceppi, M., and Pierre, P. (2009). SUnSET, a nonradioactive method to monitor protein synthesis. Nat. Methods *6*, 275–277.

Sessa, A., Fagnocchi, L., Mastrototaro, G., Massimino, L., Zaghi, M., Indrigo, M., Cattaneo, S., Martini, D., Gabellini, C., Pucci, C., et al. (2019). SETD5 regulates chromatin methylation state and preserves global transcriptional fidelity during brain development and neuronal wiring. Neuron *104*, 271–289.

Seto, E., and Yoshida, M. (2014). Erasers of histone acetylation: the histone deacetylase enzymes. Cold Spring Harb. Perspect. Biol. *6*, a018713.

Sharifi, S., and Bierhoff, H. (2018). Regulation of RNA polymerase I transcription in development, disease, and aging. Annu. Rev. Biochem. *87*, 51–73.

Sicinski, P., Donaher, J.L., Parker, S.B., Li, T., Fazeli, A., Gardner, H., Haslam, S.Z., Bronson, R.T., Elledge, S.J., and Weinberg, R.A. (1995). Cyclin D1 provides a link between development and oncogenesis in the retina and breast. Cell *82*, 621–630.

Sirmaci, A., Spiliopoulos, M., Brancati, F., Powell, E., Duman, D., Abrams, A., Bademci, G., Agolini, E., Guo, S., Konuk, B., et al. (2011). Mutations in ANKRD11 cause KBG syndrome, characterized by intellectual disability, skeletal malformations, and macrodontia. Am. J. Hum. Genet. *89*, 289–294.

Stur, E., Soares, L.A., and Louro, I.D. (2017). SETD5 gene variant associated with mild intellectual disability—a case report. Genet. Mol. Res. *16*, 2.

Szczaluba, K., Brzezinska, M., Kot, J., Rydzanicz, M., Walczak, A., Stawinski, P., Werner, B., and Ploski, R. (2016). SETD5 loss-of-function mutation as a likely cause of a familial syndromic intellectual disability with variable phenotypic expression. Am. J. Med. Genet. A *170*, 2322–2327.

Sztainberg, Y., and Zoghbi, H.Y. (2016). Lessons learned from studying syndromic autism spectrum disorders. Nat. Neurosci. *19*, 1408–1417.

Tarn, W., and Lai, M. (2011). Translational control of cyclins. Cell Div. *6*, 5.

Whetstine, J.R., Nottke, A., Lan, F., Huarte, M., Smolikov, S., Chen, Z., Spooner, E., Li, E., Zhang, G., Colaiacovo, M., et al. (2006). Reversal of histone lysine trimethylation by the JMJD2 family of histone demethylases. Cell *125*, 467–481.

Xiao, L., and Grove, A. (2009). Coordination of ribosomal protein and ribosomal RNA gene expression in response to TOR signaling. Curr. Genomics *10*, 198–205.

Yu, S.E., Kim, M.S., Park, S.H., Yoo, B.C., Kim, K.H., and Jang, Y.K. (2017). SET domain-containing protein 5 is required for expression of primordial germ cell specification-associated genes in murine embryonic stem cells. Cell Biochem. Funct. *35*, 247–253.

Zhang, Y., Yan, L., Yao, W., Chen, K., Xu, H., and Ye, Z. (2019). Integrated analysis of genetic abnormalities of the histone lysine methyltransferases in prostate cancer. Med. Sci. Monit. *25*, 193–239.

Zhou, Y., Santoro, R., and Grummt, I. (2002). The chromatin remodeling complex NoRC targets HDAC1 to the ribosomal gene promoter and represses RNA polymerase I transcription. EMBO J. *21*, 4632–4640.

iScience, Volume *23*

Supplemental Information

The Autism-Related Protein SETD5 Controls Neural Cell Proliferation through Epigenetic Regulation of rDNA Expression

Tadashi Nakagawa, Satoko Hattori, Risa Nobuta, Ryuichi Kimura, Makiko Nakagawa, Masaki Matsumoto, Yuko Nagasawa, Ryo Funayama, Tsuyoshi Miyakawa, Toshifumi Inada, Noriko Osumi, Keiichi I. Nakayama, and Keiko Nakayama

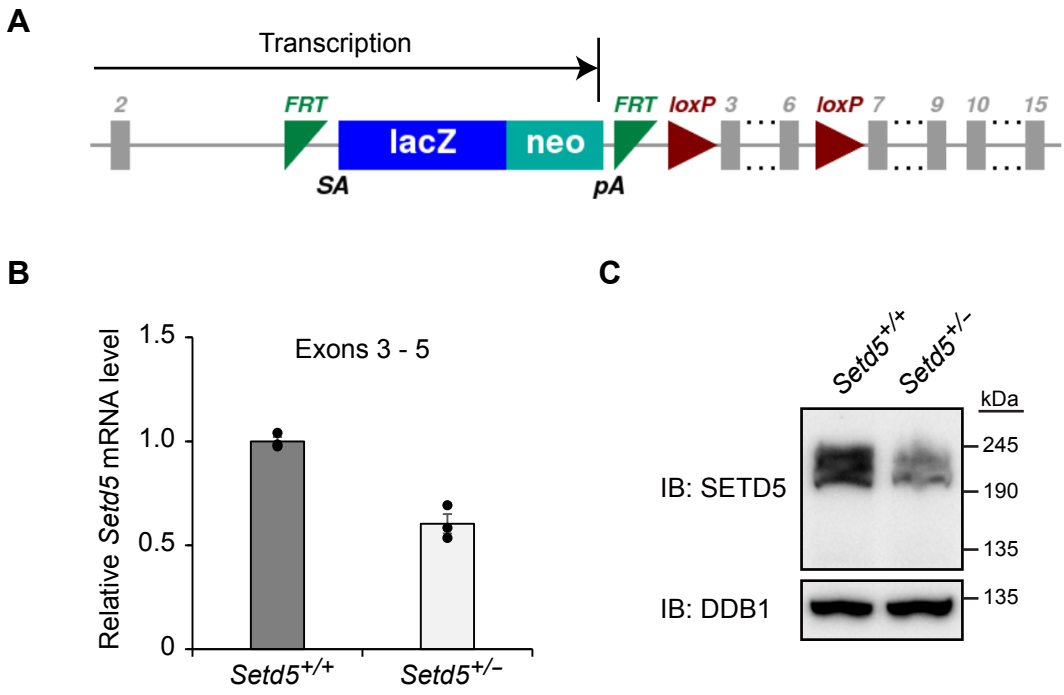
A
Transcription
2
FRT
lacZ
neo
SA
pA
FRT
loxP
3
6
loxP
7
9
10
15
B
Exons 3 - 5
Relative Setd5 mRNA level
1.5
1.0
0.5
0
Setd5+/+
Setd5+/−
C
Setd5+/+
Setd5+/−
kDa
IB: SETD5
IB: DDB1
245
190
135
135

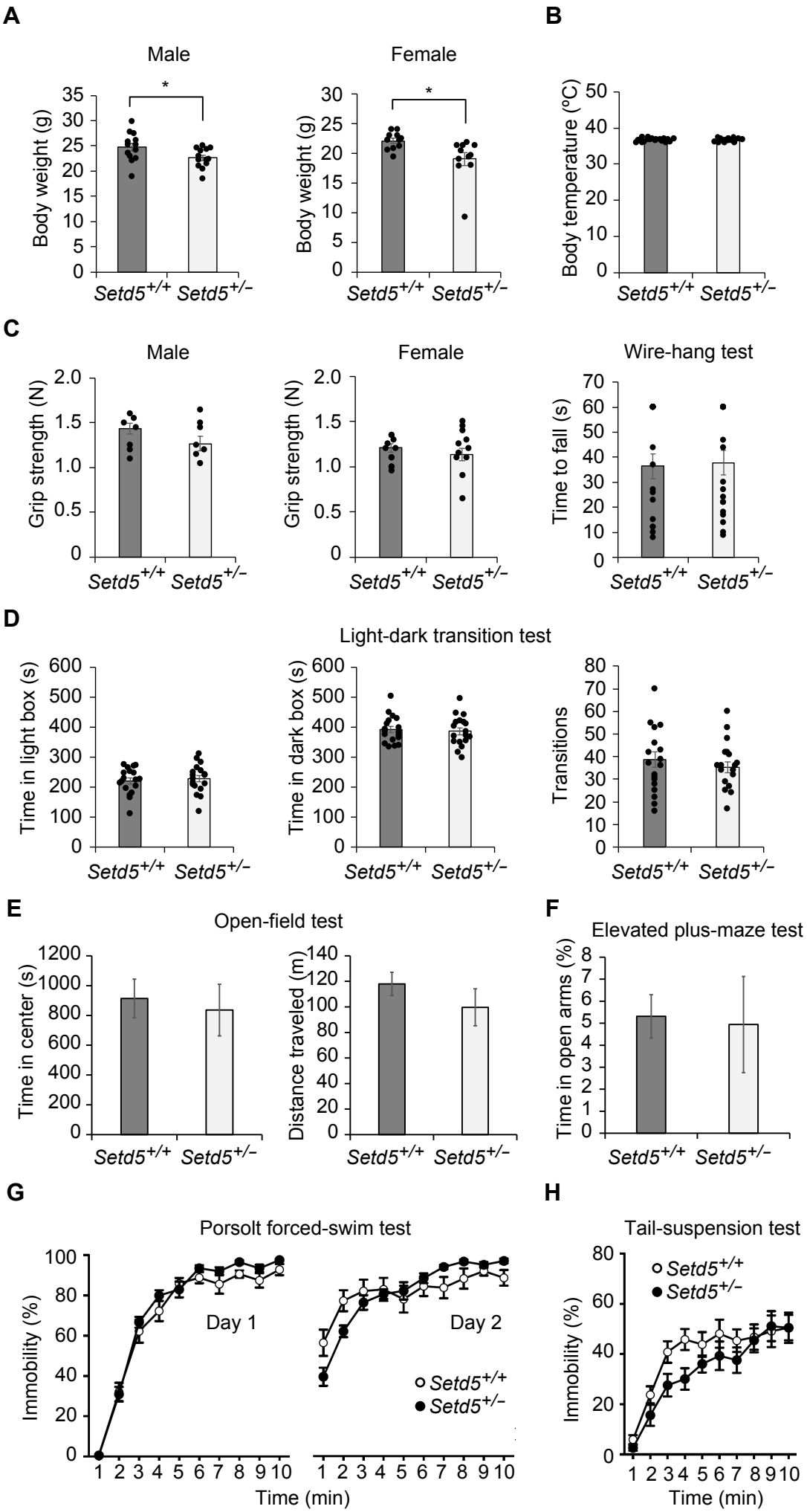
A
Male
Female
Body weight (g)
*
Setd5+/+
Setd5+/–
B
Body temperature (ºC)
C
Male
Female
Wire-hang test
Grip strength (N)
Time to fall (s)
D
Light-dark transition test
Time in light box (s)
Time in dark box (s)
Transitions
E
Open-field test
Time in center (s)
Distance traveled (m)
F
Elevated plus-maze test
Time in open arms (%)
G
Porsolt forced-swim test
Immobility (%)
Day 1
Day 2
Time (min)
H
Tail-suspension test

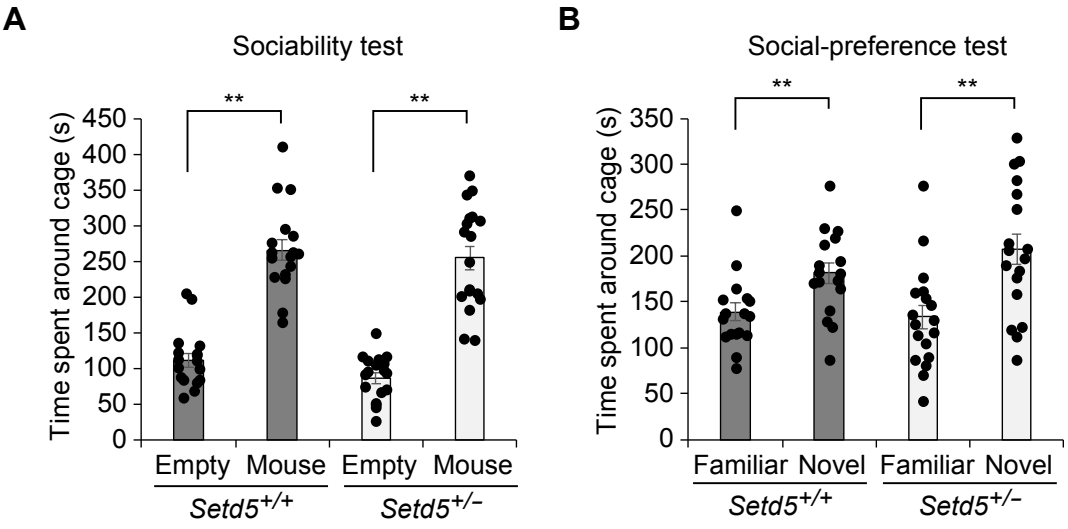
A
Sociability test
Time spent around cage (s)
450
400
350
300
250
200
150
100
50
0
**
**
Empty
Mouse
Empty
Mouse
Setd5+/+
Setd5+/−
B
Social-preference test
Time spent around cage (s)
350
300
250
200
150
100
50
0
**
**
Familiar
Novel
Familiar
Novel
Setd5+/+
Setd5+/−

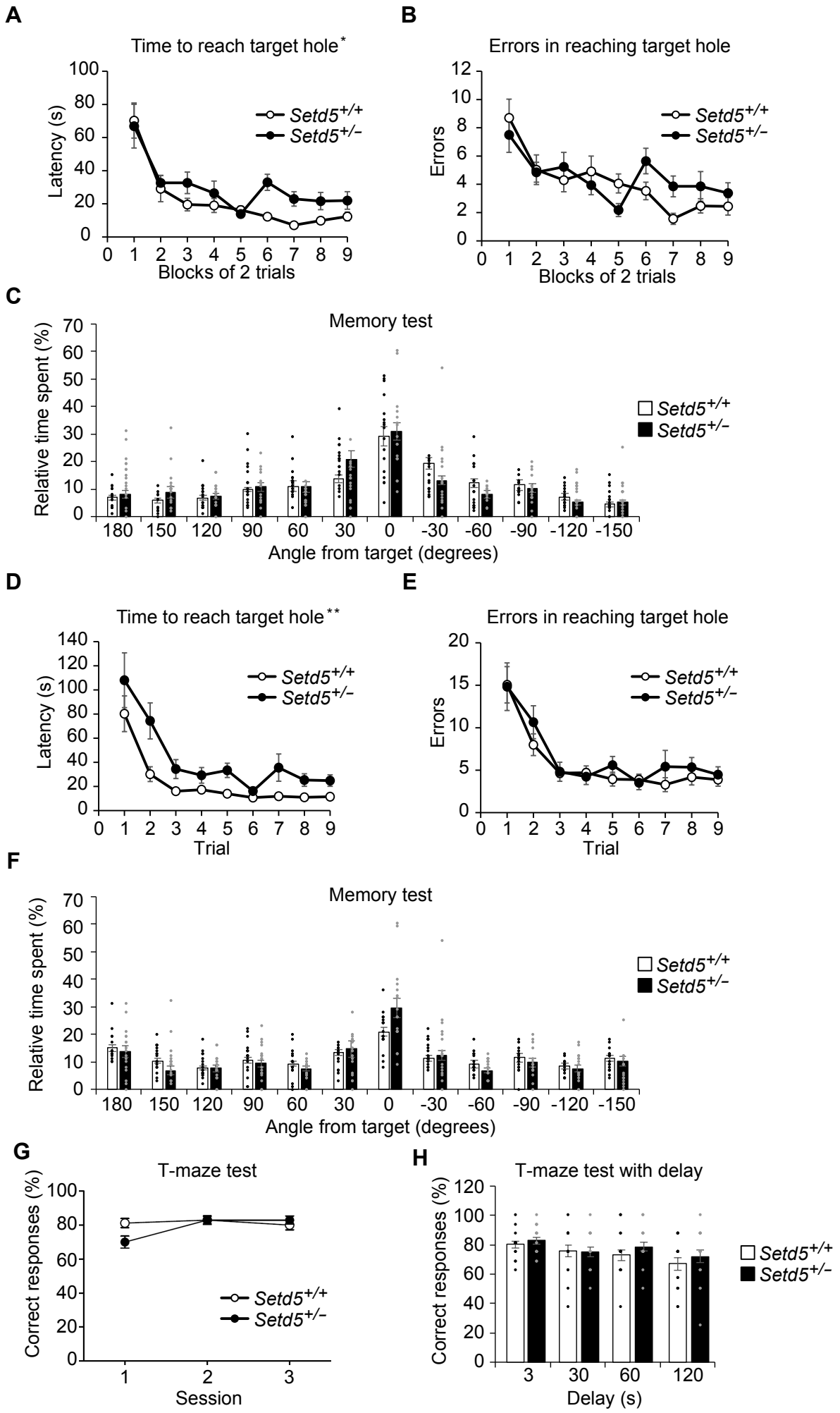
A
Time to reach target hole*
Latency (s)
Blocks of 2 trials
Setd5+/+
Setd5+/−
B
Errors in reaching target hole
Errors
Blocks of 2 trials
C
Memory test
Relative time spent (%)
Angle from target (degrees)
D
Time to reach target hole**
Latency (s)
Trial
E
Errors in reaching target hole
Errors
Trial
F
Memory test
Relative time spent (%)
Angle from target (degrees)
G
T-maze test
Correct responses (%)
Session
H
T-maze test with delay
Correct responses (%)
Delay (s)

A

Up-regulated genes in *Setd5*$^{+/-}$ brain (top 5%)

Term name	p value	FDR
GO Molecular Function		
metal ion binding	1.10E-10	6.21E-08
RNA polymerase II regulatory region sequence-specific DNA binding	2.82E-06	4.55E-04
transcription factor binding	5.63E-06	8.19E-04
core promoter binding	9.92E-06	1.21E-03
transcriptional activator activity, RNA polymerase II proximal promoter sequence-specific DNA binding	1.80E-05	1.98E-03
GO Cellular Component		
integral component of plasma membrane	6.37E-09	2.40E-06
cell junction	1.39E-05	1.31E-03
postsynaptic membrane	1.60E-05	1.44E-03
dendrite	7.46E-05	5.41E-03
caveola	1.33E-04	8.38E-03

B

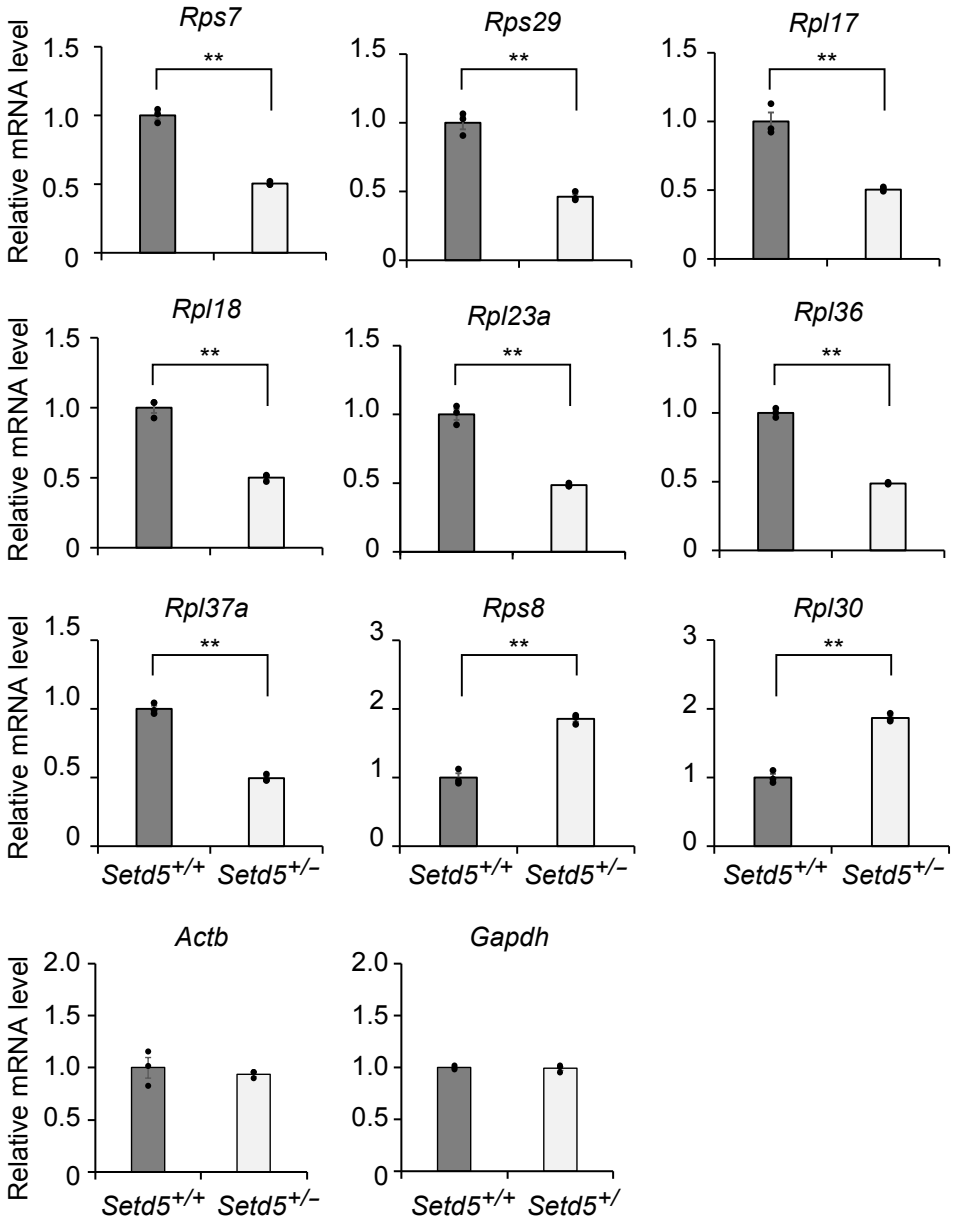

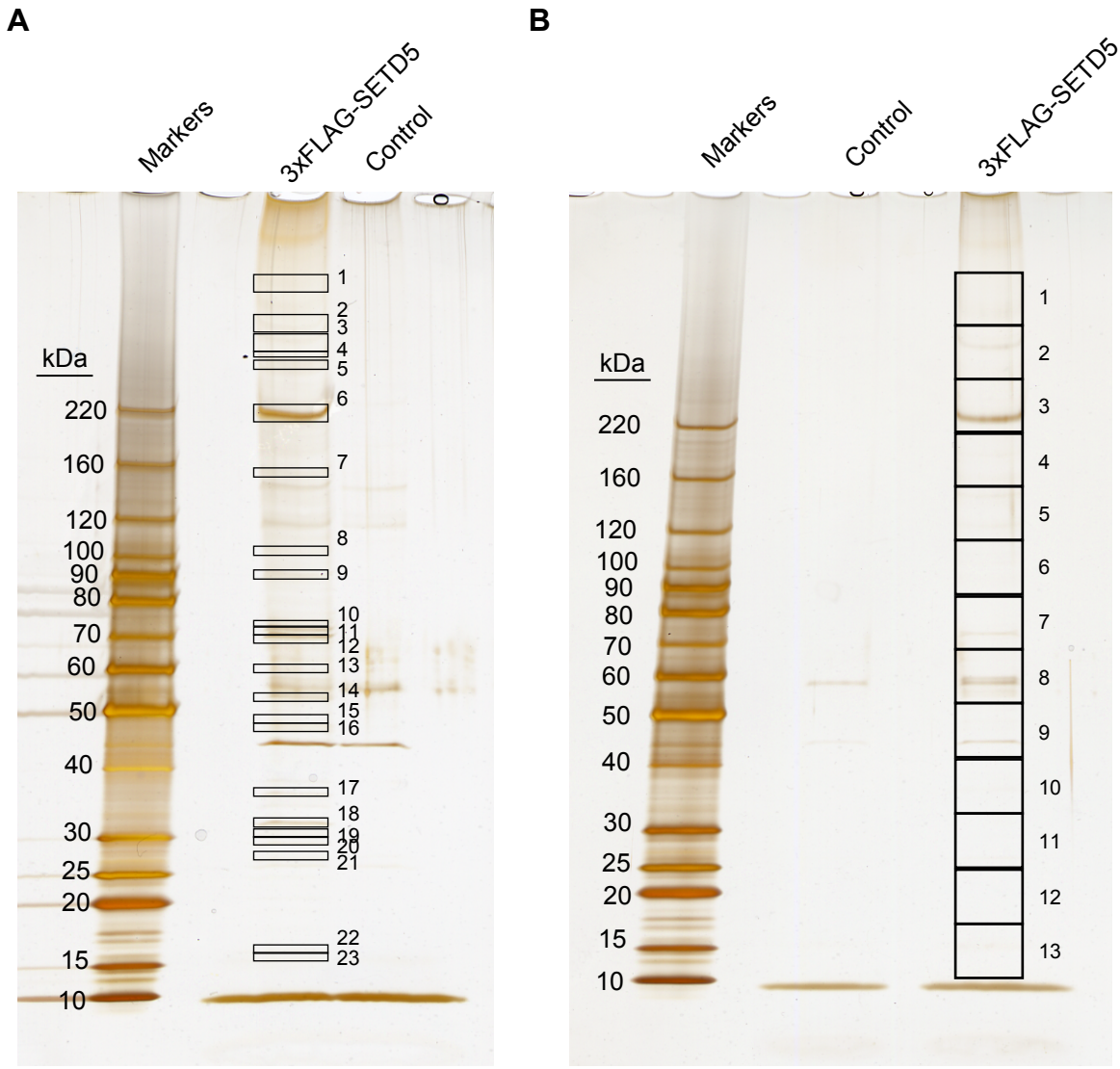
A
Markers
3xFLAG-SETD5
Control
kDa
220
160
120
100
90
80
70
60
50
40
30
25
20
15
10
1
2
3
4
5
6
7
8
9
10
11
12
13
14
15
16
17
18
19
20
21
22
23
HEK293T
B
Markers
Control
3xFLAG-SETD5
kDa
220
160
120
100
90
80
70
60
50
40
30
25
20
15
10
1
2
3
4
5
6
7
8
9
10
11
12
13
SH-SY5Y

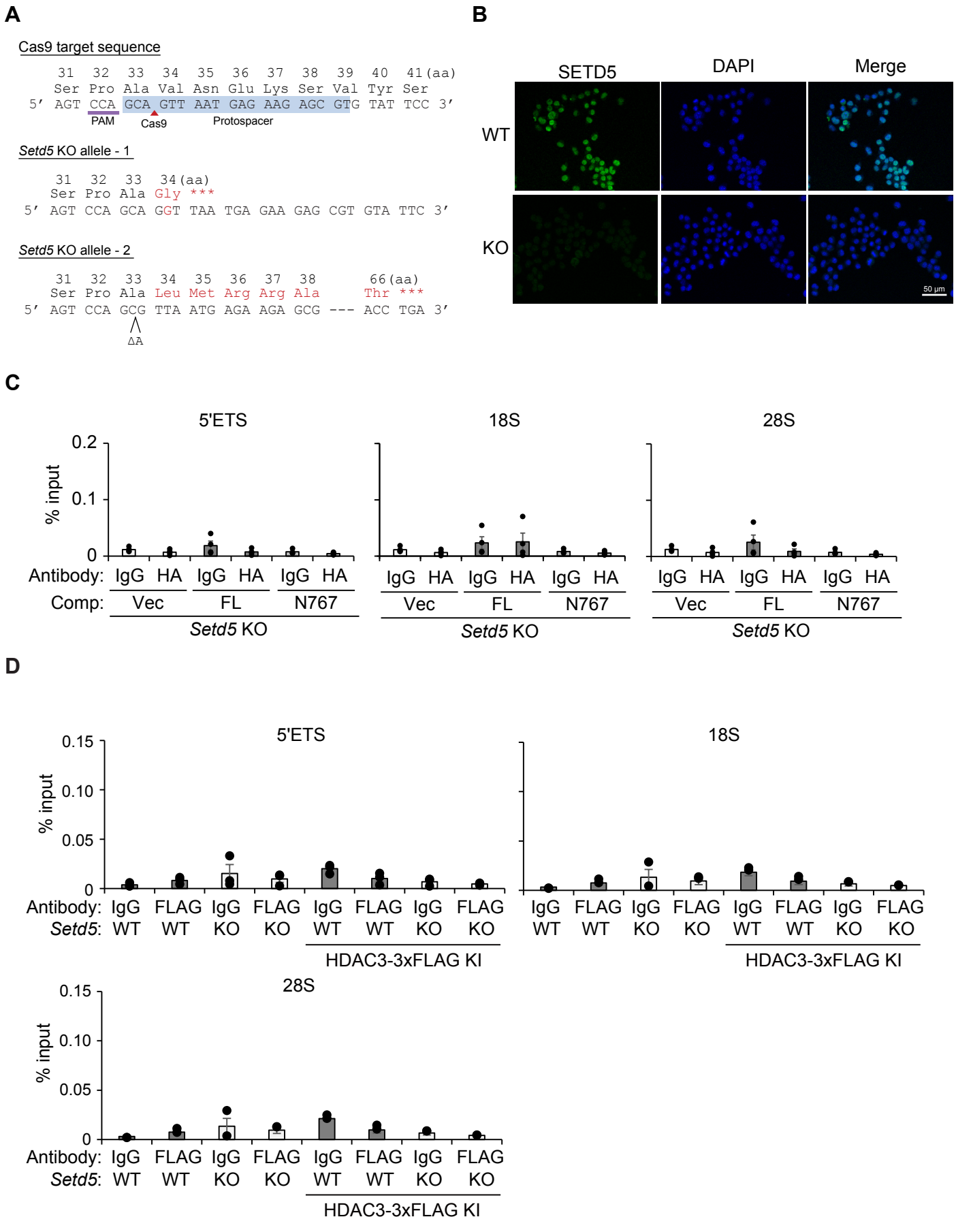
A
Cas9 target sequence
31 32 33 34 35 36 37 38 39 40 41(aa)
Ser Pro Ala Val Asn Glu Lys Ser Val Tyr Ser
5′ AGT CCA GCA GTT AAT GAG AAG AGC GTG TAT TCC 3′
PAM
Cas9
Protospacer
Setd5 KO allele - 1
31 32 33 34(aa)
Ser Pro Ala Gly ***
5′ AGT CCA GCA GGT TAA TGA GAA GAG CGT GTA TTC 3′
Setd5 KO allele - 2
31 32 33 34 35 36 37 38 66(aa)
Ser Pro Ala Leu Met Arg Arg Ala Thr ***
5′ AGT CCA GCG TTA ATG AGA AGA GCG --- ACC TGA 3′
ΔA
B
SETD5
DAPI
Merge
WT
KO
50 μm
C
5'ETS
18S
28S
% input
0.2
0.1
0
Antibody: IgG HA IgG HA IgG HA
Comp: Vec FL N767
Setd5 KO
D
5'ETS
18S
28S
% input
0.15
0.10
0.05
0
Antibody: IgG FLAG IgG FLAG IgG FLAG IgG FLAG
Setd5: WT WT KO KO WT WT KO KO
HDAC3-3xFLAG KI

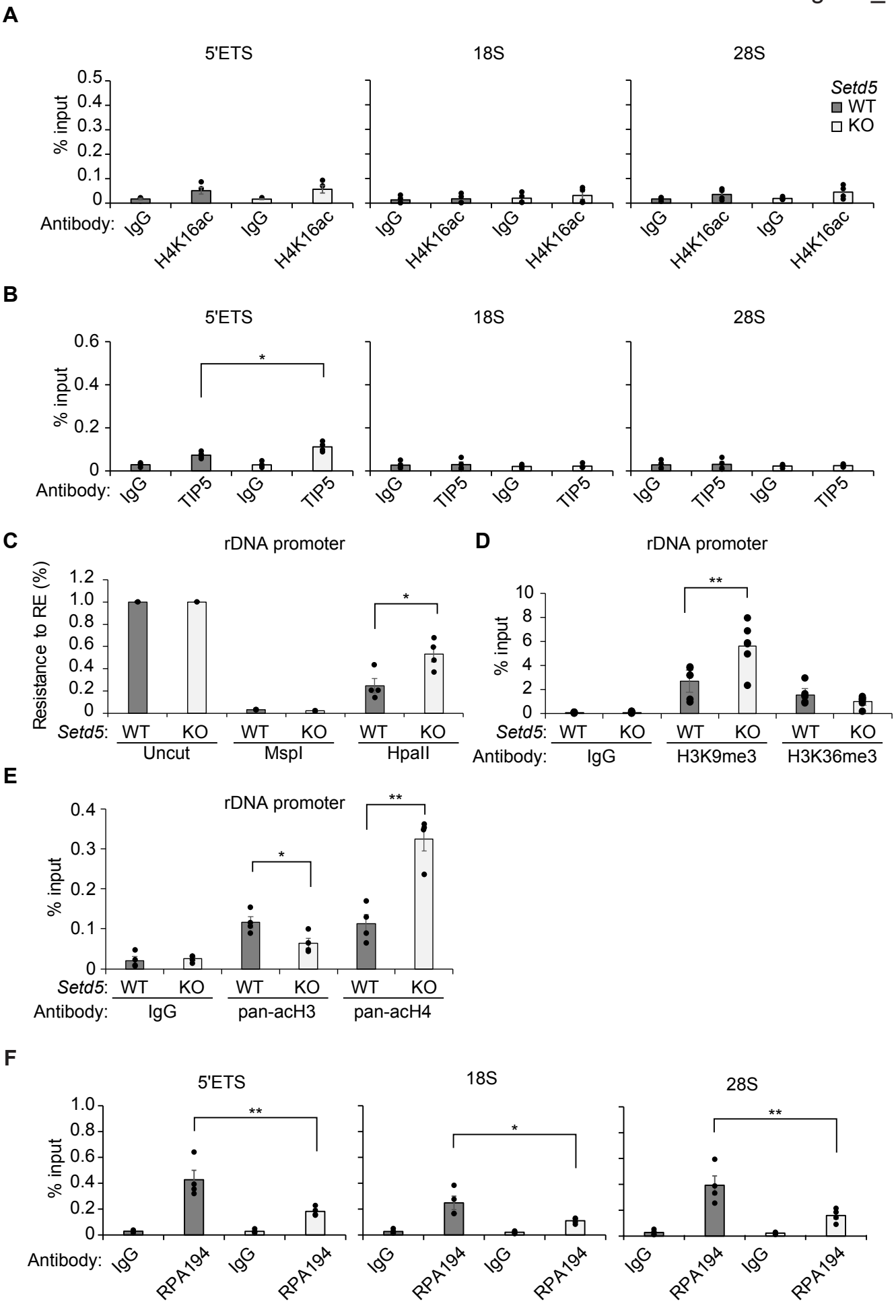
A
5'ETS
18S
28S
% input
Setd5
WT
KO
Antibody:
IgG
H4K16ac
B
TIP5
C
rDNA promoter
Resistance to RE (%)
Setd5:
Uncut
MspI
HpaII
D
H3K9me3
H3K36me3
E
pan-acH3
pan-acH4
F
RPA194

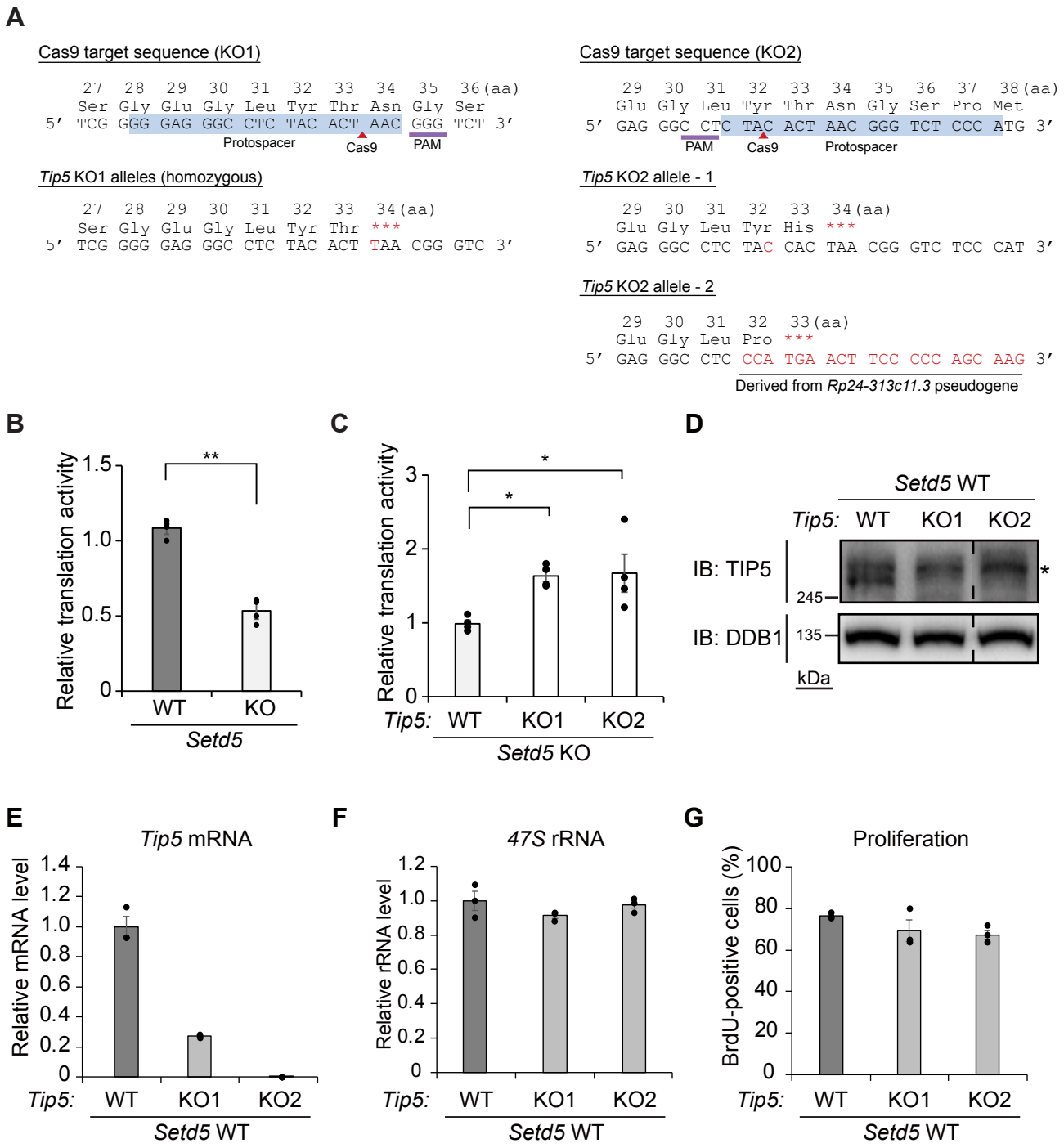
A
Cas9 target sequence (KO1)
27 28 29 30 31 32 33 34 35 36(aa)
Ser Gly Glu Gly Leu Tyr Thr Asn Gly Ser
5′ TCG GGG GAG GGC CTC TAC ACT AAC GGG TCT 3′
Protospacer
Cas9
PAM
Tip5 KO1 alleles (homozygous)
27 28 29 30 31 32 33 34(aa)
Ser Gly Glu Gly Leu Tyr Thr ***
5′ TCG GGG GAG GGC CTC TAC ACT TAA CGG GTC 3′
Cas9 target sequence (KO2)
29 30 31 32 33 34 35 36 37 38(aa)
Glu Gly Leu Tyr Thr Asn Gly Ser Pro Met
5′ GAG GGC CTC TAC ACT AAC GGG TCT CCC ATG 3′
PAM
Cas9
Protospacer
Tip5 KO2 allele - 1
29 30 31 32 33 34(aa)
Glu Gly Leu Tyr His ***
5′ GAG GGC CTC TAC CAC TAA CGG GTC TCC CAT 3′
Tip5 KO2 allele - 2
29 30 31 32 33(aa)
Glu Gly Leu Pro ***
5′ GAG GGC CTC CCA TGA ACT TCC CCC AGC AAG 3′
Derived from Rp24-313c11.3 pseudogene
B
Relative translation activity
1.5
1.0
0.5
0
**
WT
KO
Setd5
C
Relative translation activity
3
2
1
0
*
*
Tip5: WT KO1 KO2
Setd5 KO
D
Setd5 WT
Tip5: WT KO1 KO2
IB: TIP5
IB: DDB1
245
135
kDa
*
E
Tip5 mRNA
Relative mRNA level
1.4
1.2
1.0
0.8
0.6
0.4
0.2
0
Tip5: WT KO1 KO2
Setd5 WT
F
47S rRNA
Relative rRNA level
1.2
1.0
0.8
0.6
0.4
0.2
0
Tip5: WT KO1 KO2
Setd5 WT
G
Proliferation
BrdU-positive cells (%)
100
80
60
40
20
0
Tip5: WT KO1 KO2
Setd5 WT

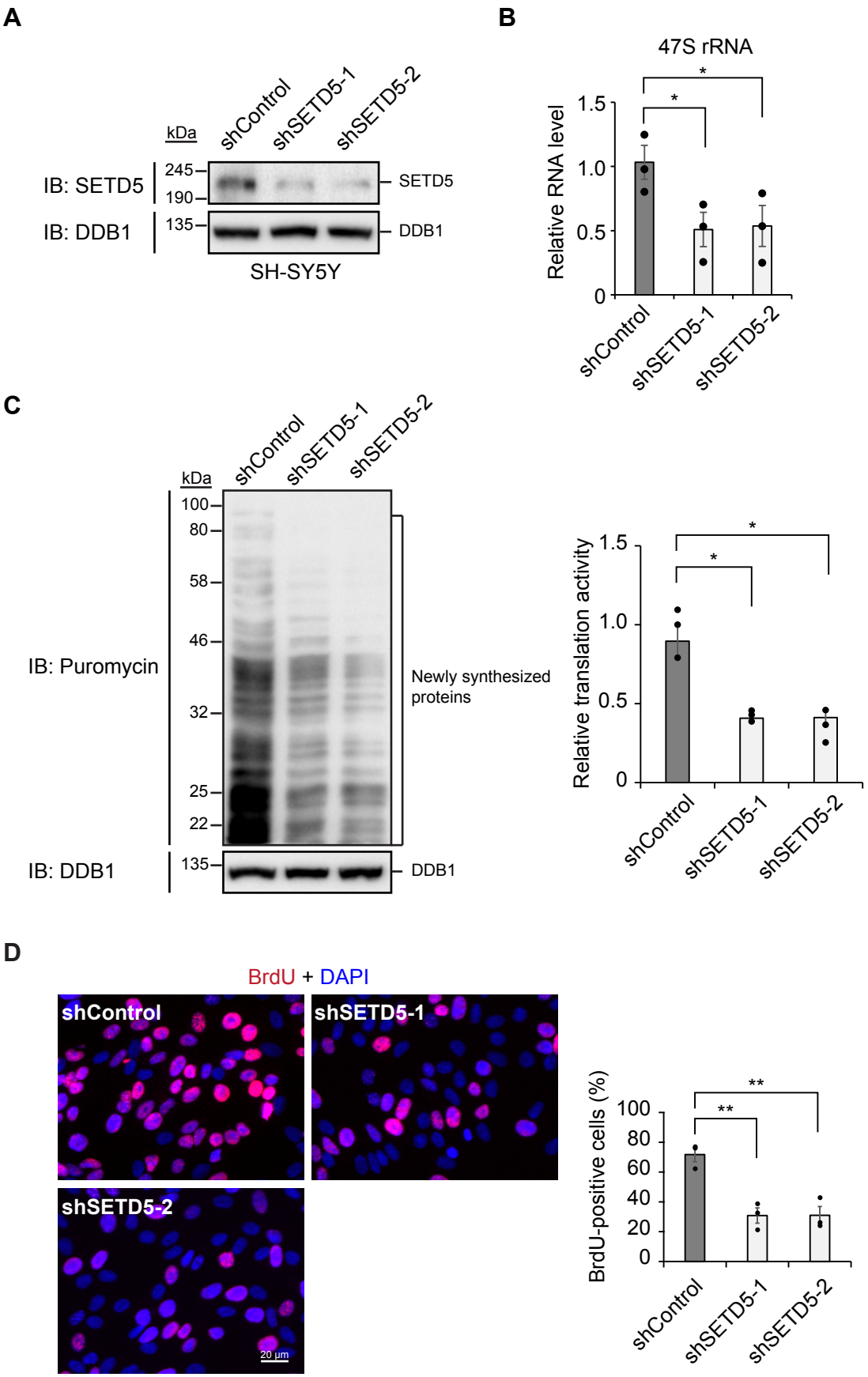
A
shControl
shSETD5-1
shSETD5-2
kDa
IB: SETD5
245
190
SETD5
IB: DDB1
135
DDB1
SH-SY5Y
B
47S rRNA
Relative RNA level
1.5
1.0
0.5
0
shControl
shSETD5-1
shSETD5-2
C
kDa
100
80
58
46
32
25
22
IB: Puromycin
Newly synthesized proteins
IB: DDB1
135
DDB1
Relative translation activity
D
BrdU + DAPI
shControl
shSETD5-1
shSETD5-2
20 μm
BrdU-positive cells (%)
100
80
60
40
20
0

SUPPLEMENTAL FIGURE LEGENDS

Figure S1. Deletion of *Setd5* in Mice, Related to Figure 1

(A) Schematic diagram of the disrupted *Setd5* allele, showing insertion of a lacZ-neo cassette flanked by FRT sequences in intron 2 as well as loxP sites flanking exons 3 to 6. Transcription is terminated by a poly(A) addition sequence (pA) located in the neo gene. SA, splicing acceptor.

(B) Reverse transcription (RT) and quantitative polymerase chain reaction (qPCR) analysis of *Setd5* mRNA in adult $Setd5^{+/+}$ or $Setd5^{+/-}$ mouse brain. PCR primers were targeted to exons 3 to 5. Data are means ± SEM (n = 3 per genotype).

(C) Immunoblot (IB) analysis of SETD5 protein and DDB1 (loading control) in adult $Setd5^{+/+}$ or $Setd5^{+/-}$ mouse brain.

Figure S2. General Health of and Absence of Anxiety- or Depression-like Behavior in $Setd5^{+/-}$ Mice, Related to Figure 1

(A) Body weight at 10 weeks of age. A significant sex difference ($p < 0.01$, one-way ANOVA) in body weight was detected, and so male and female mutant mice were compared separately with WT controls. Data are means ± SEM (n = 13 males and n = 11 females for each genotype). *$p < 0.05$ (one-way ANOVA).

(B) Body temperature at 10 weeks of age. Data are means ± SEM (n = 18 for each genotype).

(C) Grip strength and latency to falling in the wire-hang test. A significant sex difference in grip strength was detected ($p < 0.05$, one-way ANOVA), and so male and female mutant mice were compared separately with WT controls. Data are means ± SEM (total of n = 18 for each genotype).

(D) Light-dark transition test. Time spent in the light box, time spent in the dark box, and the number of light-dark transitions were measured. Data are means ± SEM (n = 18 for each genotype).

(E) Open-field test. Time spent in the center field and distance traveled were measured. Data are means ± SEM (n = 18 for each genotype).

(F) Elevated plus-maze test. Time spent in the open arms was measured. Data are means ± SEM (n = 18 for each genotype).

(G) Porsolt forced-swim test. Immobility in consecutive blocks of 1 min in trials on day 1 and day 2 was measured. Data are means ± SEM (n = 17 for each genotype).

(H) Tail-suspension test. Immobility was calculated in consecutive blocks of 1 min. Data are means ± SEM (n = 17 for each genotype).

Figure S3. Three-Chamber Tests of Sociability and Social Preference of *Setd5*$^{+/-}$ Mice, Related to Figure 1

(A) *Setd5*$^{+/+}$ or *Setd5*$^{+/-}$ mice were given access to an empty cage and a cage containing a stranger mouse of the same sex, and the time spent around each cage was measured. Data are means ± SEM (n = 17, *Setd5*$^{+/+}$; n = 18, *Setd5*$^{+/-}$). **p < 0.01 (paired t test).

(B) Test mice were given access to a cage containing a familiar mouse of the same sex and a cage containing a novel mouse of the same sex, and the time spent around each cage was measured. Data are means ± SEM (n = 17, *Setd5*$^{+/+}$; n = 18, *Setd5*$^{+/-}$). **p < 0.01 (paired t test).

Figure S4. Memory Formation in *Setd5*$^{+/-}$ Mice Assessed by the Barnes Maze Test and the T-Maze Test, Related to Figure 1

(A–C) Time spent to reach the target hole (A) and number of errors committed before reaching the target hole (B) in training trials as well as the time spent at each hole in the probe test (C) for *Setd5*$^{+/+}$ and *Setd5*$^{+/-}$ mice in the Barnes maze test. Data are means ± SEM (n = 17 for each genotype). *p < 0.05 (two-way repeated-measures ANOVA).

(D–F) Time spent to reach the target hole (D) and the number of errors committed before reaching the target hole (E) in training trials as well as the time spent at each hole

in the probe test (F) for the reversal phase of the Barnes maze test. Data are means ± SEM (n = 17 for each genotype). **p < 0.01 (two-way repeated-measures ANOVA).

(G and H) Percentage of correct responses for mice during the first three sessions (G) and during subsequent consecutive sessions with various delay times (H) in the T-maze spontaneous alternation task. Data are means ± SEM (n = 17 for each genotype).

Figure S5. Analysis of Gene Expression in the Brain of *Setd5*$^{+/-}$ Mice, Related to Figure 2

(A) GO analysis of molecular function and cellular component for the 617 genes (5%) showing the highest level of up-regulation in the *Setd5*$^{+/-}$ mouse brain compared with the WT mouse brain as performed with the PANTHER overrepresentation test (Mi et al., 2013).

(B) RT-qPCR analysis of ribosomal protein gene expression in the brain of adult *Setd5*$^{+/+}$ and *Setd5*$^{+/-}$ mice. *Actb* and *Gapdh* mRNAs were examined as internal controls. Data are means ± SEM (n = 3 for each genotype). **p < 0.01 (Student's t test).

Figure S6. Identification of Proteins Associated with SETD5, Related to Figure 3

(A) Silver staining of an SDS-PAGE gel loaded with an immunoprecipitate of 3×FLAG-SETD5 expressed in HEK293T cells. Band slices subjected to LC–MS/MS analysis are indicated.

(B) Silver staining of an SDS-PAGE gel loaded with an immunoprecipitate of 3×FLAG-SETD5 expressed in SH-SY5Y cells. Band slices subjected to LC–MS/MS analysis are indicated.

Figure S7. Generation of *Setd5* KO Neuro2a Cells and Lack of Association of SETD5 and HDAC3 with the rDNA Gene Body, Related to Figure 4

(A) Strategy for mutagenesis of mouse *Setd5* with the CRISPR/Cas9 system, and Sanger genomic sequencing results for *Setd5* KO Neuro2a cells. The protospacer sequence is highlighted in blue, the protospacer-adjacent motif (PAM) is underlined in purple, and the cleavage site is indicated by the red arrowhead. The KO cells harbor one *Setd5* allele with a 1-nucleotide insertion that results in protein truncation at amino acid (aa) position 34 and one allele with a 1-nucleotide deletion that results in a codon frameshift after codon 33.

(B) Immunofluorescence analysis of SETD5 in WT and *Setd5* KO Neuro2a cells. Nuclei were stained with DAPI. Scale bar, 50 μm.

(C) ChIP-qPCR analysis of HA-SETD5 binding to the rDNA gene body in *Setd5* KO Neuro2a cells complemented (Comp) with FL or N767 mutant forms of HA-SETD5 as in Figure 4D. ChIP was performed with antibodies to HA and with control IgG. Data are means ± SEM (n = 4 independent experiments). Scales are identical to that in Figure 4F, so that direct comparison of protein levels at the rDNA promoter and gene body is possible.

(D) ChIP-qPCR analysis of endogenous HDAC3-3×FLAG binding to the rDNA gene body in *Setd5* WT or KO Neuro2a cells engineered as in Figure 4G. ChIP was performed with antibodies to FLAG and with control IgG. Data are means ± SEM (n = 3 independent experiments). Scales are identical to that in Figure 4H, so that direct comparison of protein levels at the rDNA promoter and gene body is possible.

Figure S8. Epigenetic Modifications and Binding of TIP5 and RPA194 at rDNA in *Setd5* KO Neuro2a Cells, Related to Figure 5

(A and B) ChIP-qPCR analysis of H4K16ac (A) and TIP5 (B) at the rDNA gene body in WT or *Setd5* KO Neuro2a cells. Data are means ± SEM (n = 4 independent experiments). *p < 0.05 (one-way ANOVA followed by Tukey's test). Scales are

identical to those in Figure 5A (H4K16ac) and Figure 5B (TIP5), so that direct comparison of protein levels at the rDNA promoter and gene body is possible.

(C) DNA methylation at the rDNA promoter in WT or *Setd5* KO Neuro2a cells. Genomic DNA was cut with MspI (which is methylation insensitive) or HpaII (which is methylation sensitive), and resistance to restriction enzyme (RE) digestion was determined by qPCR amplification of the rDNA promoter region. Data are means ± SEM (n = 4 independent experiments). *p < 0.05 (Student's t test).

(D and E) ChIP-qPCR analysis of H3K9me3 and H3K36me3 (D) as well as of pan (K9+K14+K18+K23+K27)–acetylated histone 3 (pan-acH3) and pan (K5+K8+K12)–acetylated histone 4 (pan-acH4) at the rDNA promoter of WT or *Setd5* KO Neuro2a cells. Data are means ± SEM (n = 4 independent experiments). *p < 0.05, **p < 0.01 (one-way ANOVA followed by Tukey's test).

(F) ChIP-qPCR analysis of RPA194 at the rDNA gene body in WT or *Setd5* KO Neuro2a cells. Data are means ± SEM (n = 4 independent experiments). *p < 0.05, **p < 0.01 (one-way ANOVA followed by Tukey's test). Scales are identical to that in Figure 5C, so that direct comparison of protein levels at the rDNA promoter and gene body is possible.

Figure S9. Generation and Translational Activity of *Tip5;Setd5* Double-KO Neuro2a Cells as well as Generation, rDNA expression and Proliferation of *Tip5* single-KO Neuro2a Cells, Related to Figure 5

(A) Strategy for mutagenesis of mouse *Tip5* with the CRISPR/Cas9 system, and Sanger genomic sequencing results for *Tip5* KO Neuro2a cells. The protospacer sequence is highlighted in blue, the PAM is underlined in purple, and the cleavage site is indicated by the red arrowhead. *Tip5* KO1 Neuro2a cells harbor a 1-nucleotide insertion in both alleles of *Tip5* that generates a stop codon at position 34. *Tip5* KO2 Neuro2a cells harbor one allele of *Tip5* with a 1-nucleotide insertion that results in protein truncation at amino acid (aa) position 33, and one allele with an insertion likely derived from the *Rp24-313c11.3* pseudogene that generates a stop codon at position 33.

(B and C) Relative translational activity measured as in Figure 5F and 5G, respectively. Data are means ± SEM (n = 4 independent experiments). *p < 0.05, **p < 0.01 by Student's t test (E) or one-way ANOVA followed by Tukey's test (F).

(D) Immunoblot analysis of TIP5 in WT and *Tip5* KO Neuro2a cells. The Cas9 targets are the same as in *Tip5* KO cells on the *Setd5* KO background (Figure S9A). * indicates non-specific band.

(E) RT-qPCR analysis of *Tip5* mRNA. The reduction in *Tip5* mRNA abundance in the *Tip5* KO cells is most likely mediated by nonsense mRNA decay. Data are means ± SEM (n = 3 independent experiments).

(F) RT-qPCR analysis of 47S rRNA. Data are means ± SEM (n = 3 independent experiments).

(G) Cell proliferation based on BrdU staining. Data are means ± SEM (n = 3 independent experiments).

Figure S10. Depletion of SETD5 Impairs rDNA Expression, Translational Activity, and Cell Proliferation in SH-SY5Y Cells, Related to Figures 4 and 5

(A) Immunoblot analysis of SETD5 in SH-SY5Y cells infected with lentiviruses encoding doxycyclin-inducible control (shControl) or SETD5 (shSETD5-1 or -2) short hairpin RNAs.

(B) RT-qPCR analysis of 47S rRNA in cells as in (A). Data are means ± SEM (n = 3 independent experiments). *$p < 0.05$ (one-way ANOVA followed by Tukey's test).

(C) Immunoblot analysis of translational activity on the basis of puromycin incorporation into newly synthesized proteins in cells as in (A). Relative translational

activity was determined as mean ± SEM values (n = 3 independent experiments). *p < 0.05 (one-way ANOVA followed by Tukey's test).

(D) Immunofluorescence analysis of BrdU incorporation in cells as in (A). Nuclei were stained with DAPI. Scale bar, 20 μm. The percentage of BrdU-positive cells was determined for each condition as the mean ± SEM (n = 3 independent experiments). **p < 0.01 (one-way ANOVA followed by Tukey's test).

TRANSPARENT METHODS

Mouse Maintenance

Setd5$^{+/-}$ mice on the C57BL/6N background were obtained from the Wellcome Trust Sanger Institute (Bradley et al., 2012; Pettitt et al., 2009; Skarnes et al., 2011; White et al., 2013) and were maintained in a specific pathogen–free facility at the Institute of Animal Experimentation, Tohoku University Graduate School of Medicine. They were provided with water and rodent chow ad libitum and were treated according to the Standards for Humane Care and Use of Laboratory Animals of Tohoku University and the Guidelines for Proper Conduct of Animal Experiments of the Ministry of Education, Culture, Sports, Science, and Technology of Japan. The behavioral experimental protocols were approved by the Animal Care and Use Committee of Fujita Health University.

Behavioral Analyses of Mice

Setd5$^{+/-}$ mice or their WT littermates were group-housed (three or four animals per cage) in a room with a 12-h-light, 12-h-dark cycle (lights on at 0700 hours) and with access to food and water ad libitum. Behavioral tests were performed at 10 to 32 weeks of age between 0900 and 1800 hours unless indicated otherwise. Each apparatus was

cleaned with dilute sodium hypochlorite solution and 70% ethanol before testing of each animal in order to prevent bias due to olfactory cues. With the exception of the ultrasonic vocalization test, behavioral analyses were initiated with 7 male and 11 female mice of each genotype. During the analyses, one *Setd5*$^{+/-}$ mouse and one WT mouse died of unknown causes. Differences in data between male and female mice were assessed with two-way ANOVA; if the p value was <0.05, we presented the male and female results separately. Otherwise, data for the two sexes were combined. Behavioral data were obtained automatically with the use of ImageJ-based programs developed and modified by T.M. (available through O'Hara & Co.). Statistical analysis was performed with the use of StatView (SAS Institute).

Ultrasonic Vocalization

Mice at postnatal day 6 were isolated from their mother and placed in a recording chamber to record ultrasonic vocalizations over 5 min. The vocalizations were recorded through a 0.25-inch microphone and processed with a preamplifier and main amplifier (Brüel and Kjaer, Copenhagen, Denmark). Signals were filtered from 1 Hz to 100 kHz and digitized with a sampling frequency of 250 kHz, at 16 bits per sample, with the use of a 1000-Hz high-pass digital filter (model 1322A, Axon Instruments). Sound

recordings were processed with a custom Matlab program. Short-time Fourier transform analysis was performed to obtain sonograms (1024 samples/block and 1/4 overlap, resulting in a time resolution of 1.02 ms and a frequency resolution of 0.45 kHz). Frequencies of <35 kHz were filtered out to reduce background white noise and audible squeaking from females. Consecutive powers of 10 s without ultrasonic vocalizations were sampled and averaged over time to obtain a basal power spectrum, and 1.2 times the basal power spectrum was subtracted from each experimental power spectrum and frequencies with a power of less than zero were set to zero. This procedure was used to reduce the background white noise.

Wire-Hang Test

A wire-hang test apparatus (O'Hara & Co.) was used to assess balance and grip strength. The apparatus consists of a box (21.5 by 23 by 32 cm) with a wire-mesh grid (10 by 10 cm) on top that can be inverted. Mice at 10 weeks of age were placed on the wire mesh, which was then inverted, causing the animal to grip the wire. The latency to the mouse falling was recorded, with a 60-s cutoff time.

Open-Field Test

Each mouse at 10 to 11 weeks of age was placed in the corner of an open-field apparatus (40 by 40 by 30 cm, Accuscan Instruments), which was illuminated at 100 lux. Total distance traveled and time spent in the central area (20 by 20 cm) were recorded over 120 min.

Light-Dark Transition Test

The apparatus for the light-dark transition test consisted of a cage (21 by 42 by 25 cm) that was divided into two sections of equal size by a partition with a door (O'Hara & Co.). One chamber was made of white plastic and brightly illuminated, whereas the other was black and dark. Mice at 10 weeks of age were placed in the dark side and allowed to move freely between the two chambers with the door open for 10 min. The number of transitions between the two compartments and time spent in each chamber were recorded with the use of ImageLD software.

Elevated Plus-Maze Test

The apparatus consisted of two open arms (25 by 5 cm) and two enclosed arms of the same size with 15-cm-high transparent walls (O'Hara & Co.). The arms and central square were made of white plastic plates and were elevated to a height of 55 cm above

the floor. The likelihood of animals falling from the apparatus was minimized by attachment of 3-mm-high plastic ledges to the open arms. Arms of the same type were arranged on opposite sides. Each mouse at 11 weeks of age was placed in the central square of the maze (5 by 5 cm) facing one of the closed arms, and its behavior was recorded over 10 min. The percentage of time spent in the open arms was measured with the use of ImageEP software.

T-Maze Test

The spontaneous alternation task was conducted with an automatic T-maze apparatus (O'Hara & Co.) constructed of white plastic runways with 25-cm-high walls. The maze is partitioned into six areas by sliding doors that can be opened downward. The stem of the T constitutes area S2 (13 by 24 cm), and the arms of the T constitute areas A1 and A2 (11.5 by 20.5 cm). Areas P1 and P2 correspond to connecting passageways from the respective arms (area A1 or A2) to the start compartment (area S1). Mice were subjected to a spontaneous alternation protocol for 3 days (one session consisting of 10 trials per day; cutoff time, 50 min). Each trial had first and second runs. On the first run, the mouse was forced to choose one of the arms of the T (area A1 or A2). After the mouse stayed for >10 s, the door that separated the arm (area A1 or A2) and the

connecting passageway (area P1 or P2) would be opened, and the mouse could return to the starting compartment (area S1) via the connecting passageway. After a 3-s delay in area S1, the mouse was given a free choice between the two T arms. The percentage of trials in which mice entered the arm opposite to that of the forced-choice run during the free-choice run was calculated. The location of the first arm (left or right) was changed in a pseudorandom manner across trials so that mice received equal numbers of left and right presentations. On days 4 to 7, a delay of 3, 30, 60, or 120 s, respectively, between the first and second runs of each trial was applied. Data acquisition, control of the sliding doors, and data analysis were performed with ImageTM software.

Social-Interaction Test in a Novel Environment

Two mice of the same sex and genotype at 11 weeks of age that had been housed in different cages were placed together in a box (40 by 40 by 30 cm) and allowed to explore freely for 10 min. Analysis was performed automatically with the use of ImageSI software. Images were captured at a rate of three frames per second. Mean duration per contact and total duration per contact were recorded by the software.

Sociability and Social-Novelty Preference Test

The testing apparatus consisted of a rectangular, three-chambered box with a lid fitted with a video camera (O'Hara & Co.). Each chamber measured 20 by 40 by 47 cm, and the dividing walls were made of clear Plexiglas and had a small rectangular opening (5 by 3 cm) that allowed access into each chamber. Small round wire cages (11 cm in height, with a bottom diameter of 9 cm and vertical bars 0.5 cm apart) were located in corners of the left and right chambers. The subject mouse was first placed in the middle chamber and allowed to explore the entire test box for 10 min. It was then immediately transferred to a clean holding cage, and an unfamiliar mouse of the same sex (stranger 1) that had had no prior contact with the subject mouse was placed in one of the side cages. The location of stranger 1 in the left versus right side chamber was systematically alternated between trials. The cage containing the stranger mouse allowed nose contact with the subject mouse between the bars but prevented fighting. The subject mouse was then returned to the middle chamber and allowed to explore for 10 min (sociability test). The amount of time spent around each cage was measured with the aid of the camera fitted on top of the box in order to quantify sociability with regard to stranger 1. After the sociability test, the subject mouse was again transferred to the holding cage, and a second unfamiliar mouse of the same sex (stranger 2) was placed in the cage that had been empty during the first session. The test mouse was then returned to the middle

chamber and had a choice between the first, already-investigated unfamiliar mouse (stranger 1) and the novel unfamiliar mouse (stranger 2). The amount of time spent around each cage during a second 10-min session was measured as before (social-novelty preference test). All the mice used in these tests were 12 weeks of age. Data acquisition and analysis were performed automatically with the use of ImageCSI software.

Social-Preference Test

This test was conducted in a manner similar to that for the sociability and social-novelty preference tests. An unfamiliar mouse of the same sex and genotype (stranger) that had had no prior contact with the subject mouse as well as a cage mate of the subject mouse were placed in the cages of the side chambers. The test mouse thus had a choice between an unfamiliar mouse (stranger) and a familiar mouse (cage mate). All the mice used in this test were 47 to 50 weeks of age.

Barnes Maze Test

The Barnes maze test was performed on "dry land," a white circular surface with a diameter of 1.0 m and with 12 holes equally spaced around the perimeter (O'Hara &

Co.). The circular open field was elevated 75 cm from the floor. A black Plexiglas escape box (17 by 13 by 7 cm) containing paper cage-bedding on its floor was located under one of the holes. The hole above the escape box represented the target, analogous to the hidden platform in the Morris task. The location of the target was consistent for a given mouse but was randomized across mice. The maze was rotated daily, with the spatial location of the target unchanged with respect to visual room cues, in order to prevent bias based on olfactory or proximal cues within the maze. One or two trials per day were conducted. A probe trial was performed without the escape box at 1 day after the last training trial to confirm that this spatial task was dependent on navigation based on distal environmental cues in the room. The location of the target for each mouse was then shifted to the opposite side of the circular surface, and the same protocol for training and probe trials was followed. All the mice used in this test were 15 to 19 weeks of age. Behavior was recorded with the use of ImageBM software.

Porsolt Forced-Swim Test

A transparent plastic cylinder (20 cm in height with a diameter of 10 cm) filled with water (21°–23°C) up to a height of 7.5 cm was placed in a white plastic chamber (32 by 44 by 49 cm) (O'Hara & Co.). The mouse was placed in the cylinder, and the time

during which the animal was immobile was recorded over a 10-min test period. Images were captured at two frames per second. For each pair of successive frames, the area (pixels) within which the mouse moved was measured. When the area was below a certain threshold, the mouse behavior was classified as "immobility." When the area equaled or exceeded the threshold, the mouse was classified as "moving." The optimal threshold for the classification was determined on the basis of human observation. Immobility lasting for <2 s was not included in the analysis. Data acquisition and analysis were performed automatically with ImagePS software.

Tail-Suspension Test

Mice were suspended 30 cm above the floor of a white plastic chamber (39 by 32 by 44 cm) (O'Hara & Co.) in a visually isolated area by adhesive tape placed ~1 cm from the base of the tail, and behavior was recorded over a 10-min test period. Images were captured at two frames per second. Similar to the Porsolt forced-swim test, immobility was judged by the application program according to a certain threshold. Immobility lasting for <2 s was not included in the analysis. Data acquisition and analysis were performed automatically with ImageTS software.

Cued Fear-Conditioning Test

Each mouse was placed in a transparent acrylic chamber (33 by 25 by 28 cm) with a stainless-steel grid floor made of rods 0.2 cm in diameter spaced 0.5 cm apart (O'Hara & Co.). The chamber was illuminated at 100 lux, and the mouse was allowed to explore freely for 2 min. White noise of 55 dB, which served as the conditioned stimulus (CS), was presented for 30 s, followed by a mild foot shock (0.3 mA for 2 s), which served as the unconditioned stimulus (US). Two more CS-US pairings were presented with a 2-min interstimulus interval. One day after conditioning, a cued test with altered context was conducted in a triangular box (33 by 29 by 32 cm) that was made of white Plexiglas and located in a different room. The chamber was illuminated at 30 lux. The mouse was allowed to explore the chamber for 180 s, after which the CS was presented for 180 s. Data acquisition, control of stimuli (white noise and foot shock), and data analysis were performed automatically with ImageFC software. Images were captured at one frame per second. For each pair of successive frames, the area (pixels) in which the mouse moved was measured. When this area was below a certain threshold, the behavior was judged as "freezing." When the area equaled or exceeded the threshold, the behavior was considered to be "nonfreezing." The optimal threshold (number of pixels) for such

classification was determined on the basis of human observation. Freezing that lasted for less than the defined time threshold (2 s) was not included in the analysis.

Home cage monitoring

For monitoring of behavior in a familiar environment, two genetically identical mice that had been housed separately were placed together in a home cage (29 by 18 by 12 cm). The social behavior was then monitored for 7 days with a video camera, the output of which was fed into a computer. Images were captured at a rate of one frame per second with ImageHA software.

Immunofluorescence Staining of Mouse Brain

The embryonic brain was dissected, immersed overnight in 1% paraformaldehyde in phosphate-buffered saline (PBS), and transferred to 15% sucrose in PBS overnight and then to 30% sucrose in PBS for at least 2 days for cryoprotection. The brain tissue was frozen in Tissue-Tek OTC compound (Miles) and cut into 10-μm-thick sections with a cryostat (Leica Microsystems). The cryostat sections were incubated with primary antibodies at 4°C for 16 h. After two washes with PBS containing 0.1% Tween-20 (PBS-T), the sections were incubated with AlexaFluor-conjugated secondary antibodies

at room temperature for 45 min, washed twice with PBS-T and twice with PBS, and mounted with the use of SlowFade Gold antifade reagent with DAPI (Thermo Fisher Scientific). Fluorescence signals were detected with a BZ-9000 microscope (Keyence).

Cell Culture

HEK293T (ATCC, CRL-3216), SH-SY5Y (ATCC, CRL-2266), Neuro2a (ATCC, CCL-131), and Plat-E (Gift from Toshio Kitamura' lab) cells were cultured under 5% CO_2 at 37°C in Dulbecco's modified Eagle's medium supplemented with 10% fetal bovine serum, penicillin (50 U/ml), streptomycin (50 μg/ml), 2 mM L-glutamine, 1% MEM–nonessential amino acids, and 1% sodium pyruvate (Thermo Fisher Scientific).

Cell Transfection

HEK293T and Neuro2a cells were transfected with expression plasmids with the use of polyethylenimine (Polysciences) or Lipofectamine 2000 (Thermo Fisher Scientific), respectively. For retrovirus-mediated gene transfer, Plat-E cells were transfected with retroviral vectors (pMX). For lentivirus-mediated gene transfer, HEK293T cells were transfected with lentiviral vectors (pSLIK, Addgene #25735), psPAX2 (Addgene #12260), and pMD2.G (Addgene #12259) (Shin et al., 2006). Retrovirus- or lentivirus-

containing medium was collected 48 h after transfection and supplemented with polybrene (Sigma) at 4 μg/ml. Neuro2a or SH-SY5Y cells were infected for 24 h by exposure to the virus-containing medium. Selection was performed with puromycin or G418. SH-SY5Y cells infected with lentiviruses were exposed to doxycycline (1 μg/ml) for 2 days (for overexpression of 3×FLAG-SETD5) or 5 days (for knockdown of endogenous SETD5). miRNA targeting sequences for human SETD5 knockdown are GCUUCUGGAUUUGGGCAAACA and GGAGAAAGCUGUAAAUCUUGU.

Establishment of *Setd5* and *Tip5* KO Cells

Frameshift mutations in *Setd5* or *Tip5* were induced by introduction of pSpCas9(BB)-2A-Puro–based plasmids (Addgene #48139) into Neuro2a cells by transient transfection (Ran et al., 2013). The cells were then cloned by limiting dilution in 96-well plates, and the resulting single cell–derived clones were screened for frameshift mutations by genomic PCR and sequencing. Protospacer sequences targeted by SpCas9 are as follows; ACGCTCTTCTCATTAACTGC for mouse Setd5, GGGAGGGCCTCTACACTAAC and TGGGAGACCCGTTAGTGTAG for mouse Tip5.

Generation of HDAC3-3×FLAG Knock-in Cells

A targeting vector (pBS-mHDAC3-3FLAG-KI TV) was constructed by PCR-mediated cloning of the 1-kbp region immediately upstream of the stop codon of mouse *Hdac3* (left arm) and the 1-kbp region immediately downstream of the stop codon (right arm), followed by insertion of these fragments into the pBS-3FLAG-LNL (loxP-neo-loxP) vector. Neuro2a cells were transfected with the linearized targeting vector and pSpCas9-HDAC3, which induces the formation of double-strand breaks in the 3' untranslated region of *Hdac3*. After selection in the presence of G418 (1000 μg/ml) for 7 days, the cells were transfected with pMX-puro-Cre, selected with puromycin (5 μg/ml) for 2 days, and then cloned by limiting dilution in 96-well plates. The resulting single cell–derived clones were screened for biallelic 3×FLAG knock-in by genomic PCR and sequencing as well as by immunoblot analysis.

Plasmids

A cDNA encoding SETD5 was amplified from HEK293T cells, cloned into pENTR (Thermo Fisher Scientific), and verified by sequencing. The pENTR plasmid was recombined with destination plasmids (Nakagawa et al., 2015) with the use of LR

clonase II (Thermo Fisher Scientific). Deletion mutants were prepared by PCR-based mutagenesis.

RNA Isolation and RT-qPCR Analysis

RNA was isolated with the use of an SV Total RNA Isolation System (Promega), and it was subjected to RT with a PrimeScript RT reagent kit (Takara Bio) followed by real-time PCR analysis with a StepOnePlus Real Time PCR System (Life Technologies) and Fast SYBR Green Master Mix (Life Technologies). Data were analyzed according to the $2^{-\Delta\Delta Ct}$ method and were normalized by the amount of *Cul1* mRNA. Oligonucleotide sequences of RT-qPCR primers are presented in Table S4.

RNA-seq Analysis

Total RNA was extracted from the hemispheres of 2-month-old female littermates (*Setd5*$^{+/+}$ and *Setd5*$^{+/-}$, n = 1 for each genotype) for RNA-seq analysis. RNA-seq libraries were prepared with a TruSeq Standard mRNA LT Sample Prep Kit (Illumina). Libraries were clonally amplified in the flow cell of an Illumina HiSeq 2500 instrument and sequenced (51-nucleotide paired end). Paired-end reads were mapped to the mouse genome (UCSC mm9 and RefSeq) with TopHat (Trapnell et al., 2009). Cufflinks was

used to estimate gene expression level on the basis of FPKM (Trapnell et al., 2013). FPKM data are presented in Table S2. GO analysis of molecular function and cellular component for the 617 (5%) most up-regulated or down-regulated genes in the *Setd5*$^{+/-}$ mouse brain was performed with the use of the PANTHER overrepresentation test (Mi et al., 2013). No statistics were applied to identify the most up- and down-regulated genes.

Immunoprecipitation and Immunoblot Analysis

With the exception of cell lysis for the identification of SETD5 binding proteins, cells were lysed for immunoprecipitation at 4°C for 10 min in NP-40 lysis buffer [0.5% Nonidet P-40, 50 mM Tris-HCl (pH 7.5), 150 mM NaCl, 10% glycerol, aprotinin (10 μg/ml), leupeptin (10 μg/ml), 1 mM phenylmethylsulfonyl fluoride (PMSF), 0.4 mM sodium orthovanadate, 0.4 mM EDTA, 10 mM NaF, 10 mM sodium pyrophosphate]. Crude lysates were cleared of debris by centrifugation at 20,000 × *g* for 15 min at 4°C, and the resulting supernatants were incubated with Dynabeads Protein G (Thermo Fisher Scientific) that had been conjugated with appropriate antibodies. The immune complexes were washed three times with wash buffer (0.1% Triton X-100 and 10% glycerol in PBS) and then subjected to SDS–polyacrylamide gel electrophoresis

(PAGE) followed by immunoblot analysis with appropriate antibodies. For direct immunoblot analysis of cultured cells, total cell extracts were prepared with RIPA buffer [50 mM Tris-HCl (pH 8.0), 0.1% SDS, 150 mM NaCl, 1% Nonidet P-40, 0.5% sodium deoxycholate] and cleared of debris by centrifugation at 20,000 × *g* for 15 min at 4°C. The resulting supernatants were subjected to SDS-PAGE. For immunoblot assay of embryonic and adult mouse brains, extracts were prepared by homogenization of tissue in a solution containing 50 mM Tris-HCl (pH 7.5), 250 mM sucrose, 1 mM EDTA, a protease inhibitor cocktail, and phosphatase inhibitor cocktail [(0.4 mM Sodium orthovanadate (Wako), 0.4 mM EDTA (Dojindo), 10 mM NaF (Wako) and 10 mM sodium pyrophosphate (Sigma)]. The homogenate was then mixed with an equal volume of 2× radioimmunoprecipitation assay (RIPA) buffer. Band intensities were quantified with Image J software.

Puromycin Incorporation Assay

Cells were treated with puromycin (20 μg/ml) for 30 min before lysis for immunoblot analysis with antibodies to puromycin.

Identification of SETD5 Binding Proteins by LC–MS/MS

HEK293T or SH-SY5Y cells expressing 3×FLAG-SETD5 were lysed in digitonin buffer [1% digitonin, 150 mM NaCl, 50 mM Tris-HCl (pH 7.4), aprotinin (10 μg/ml), leupeptin (10 μg/ml), 1 mM PMSF, 0.4 mM sodium orthovanadate, 0.4 mM EDTA, 10 mM NaF, 10 mM sodium pyrophosphate] and then subjected to immunoprecipitation as described above with antibodies to FLAG. After three washes with wash buffer (0.1% Triton X-100 and 10% glycerol in PBS), the immunoprecipitated proteins were eluted with elution buffer [0.1% Triton X-100, 10% glycerol, and 3×FLAG peptide (500 μg/ml) in PBS] and subjected to SDS-PAGE on a 4% to 20% gradient gel followed by silver staining. The gel was cut into slices as indicated in Figure S6, and proteins in each gel slice were digested with trypsin. The obtained peptides were dried, dissolved in a solution containing 0.1% trifluoroacetic acid and 2% acetonitrile, and then subjected to nanoscale LC and MS/MS analysis with a system consisting of an LTQ mass spectrometer (Thermo Fisher Scientific) coupled with a nanoLC instrument (Paradigm MS4, Michrom BioResources) and HTC-PAL autosampler (CTC Analytics). Peptide separation was performed with an in-house pulled fused-silica capillary packed with 3-μm C18 L-column resin (Chemicals Evaluation and Research Institute, Japan). The mobile phases consisted of 0.1% formic acid/2% acetonitrile and 0.1% formic acid/90% acetonitrile, and peptides were eluted with a linear gradient. Collision-induced

dissociation spectra were acquired automatically in the data-dependent scan mode with the dynamic exclusion option. The peak lists were generated by MSn.exe (Thermo Fisher Scientific) with a minimum scan/group value of 1 and were compared with the ipi_HUM_NEW database with the use of the MASCOT algorithm (ver. 2.4.1). Identified peptides are presented in Table S3.

Gel Filtration

Cell lysates (500 µl) prepared with NP-40 lysis buffer containing 250 U of benzonase (Novagen) were subjected to gel filtration on Superose 6 10/300 GL (GE Healthcare) with the use of an AKTA Purifier (GE Healthcare) LC system. Elution was performed with PBS at a flow rate of 0.5 ml/min. Fractions (1 ml) were collected from 6 to 17 ml and were subjected to immunoblot analysis. Approximate molecular size was calculated after calibration of the column with a Gel Filtration Calibration Kit LMW HMW (GE Healthcare).

ChIP Analysis

Cells were fixed with 1% paraformaldehyde for 10 min, exposed to glycine at a final concentration of 0.125 M in PBS to terminate fixation, and centrifuged at 1000 × *g* for 2

min at 4°C. The cell pellets were suspended in 500 μl of nuclear extraction buffer [50 mM Tris-HCl (pH 7.4), 10 mM potassium acetate, 15 mM magnesium acetate, 1% Nonidet P-40, aprotinin (10 μg/ml), leupeptin (10 μg/ml), 1 mM PMSF], incubated for 15 min on ice, and centrifuged again at 1000 × *g* for 5 min at 4°C. The resulting pellets were suspended in 500 μl of Buf NUC solution [15 mM HEPES-NaOH (pH 7.5), 60 mM KCl, 15 mM NaCl, 0.32 mM sucrose, aprotinin (10 μg/ml), leupeptin (10 μg/ml), 1 mM PMSF], mixed with 1.5 μl of 1 M $CaCl_2$, and digested with 2000 U of micrococcal nuclease (New England Biolabs) for 20 min at 37°C. After the addition of 500 μl of 2× sonication buffer [90 mM HEPES-NaOH (pH 7.8), 220 mM NaCl, 10 mM EDTA, 1% Nonidet P-40, 0.2% sodium deoxycholate, 0.2% SDS] to stop the reaction, the suspension was subjected to ultrasonic treatment with the use of a Cosmo Bio Bioruptor UCD-250 (seven cycles of 30 s on and 30 s off, level H) and then centrifuged at 13,000 × *g* for 5 min at 4°C. The resulting supernatants were incubated with rotation overnight at 4°C with the indicated antibodies conjugated to magnetic beads. Bead-bound proteins were washed consecutively with buffer A [20 mM Tris-HCl (pH 8.0), 150 mM NaCl, 1 mM EDTA, 1% Triton X-100, 0.1% sodium deoxycholate, 0.1% SDS], buffer B [20 mM Tris-HCl (pH 8.0), 500 mM NaCl, 1 mM EDTA, 1% Triton X-100, 0.1% sodium deoxycholate, 0.1% SDS], buffer C [20 mM Tris-HCl (pH 8.0), 250 mM LiCl, 1 mM

EDTA, 0.5% Nonidet P-40, 0.5% sodium deoxycholate], and Tris-EDTA buffer, and they were then eluted by consecutive exposure to RNase A (100 µg/ml) for 30 min at 50°C, proteinase K (200 µg/ml) for 30 min at 50°C, and 350 mM NaCl overnight at 65°C, each of which was dissolved in ChIP elution buffer [50 mM Tris-HCl (pH 8.0), 1 mM EDTA, 1% SDS]. After incubation of the samples with proteinase K (200 ug/ml) for 60 min at 50°C, DNA was purified with the use of AMpure XP beads in 2.5 M NaCl containing 20% polyethylene glycol, washed with 80% ethanol, eluted with EB buffer (Qiagen), and subjected to real-time PCR analysis. Oligonucleotide sequences of primers for real-time PCR analysis are presented in Table S4.

Analysis of DNA Methylation at the rDNA Promoter

CpG methylation was assayed by digestion with HpaII (a methylation-sensitive restriction enzyme) and MspI (a methylation-insensitive restriction enzyme) (Murano et al., 2014; Santoro et al., 2002). Genomic DNA (500 ng) was digested with 20 U of HpaII or MspI for 1 h at 37°C, and resistance to the restriction enzymes was determined by qPCR analysis with the primer set 5'-AAGCCCTCTCTGTCCCTGTCAC-3' and 5'-GGAGAACTGATAAGACCGACAGGT-3'.

BrdU Incorporation Assay

Cells exposed to 10 μM BrdU for 24 h were fixed with 1% paraformaldehyde, permeabilized with 0.5% Triton X-100 in PBS, denatured with 2 M HCl, washed with PBS-T, and exposed to 1% bovine serum albumin in PBS before incubation with antibodies to BrdU. The cells were then washed with PBS-T, incubated with AlexaFluor 555–labeled secondary antibodies (Thermo Fisher Scientific), washed again with PBS-T, treated with DAPI (1 μg/ml), and examined with a BZ-9000 microscope (Keyence).

Cell Cycle Profiling

Neuro2a cells (1×10^5) were incubated with 10 μM BrdU for 30 min, fixed with ice-cold 70% ethanol for 30 min, and treated with a denaturing solution (2 M HCl containing 0.5% Triton X-100) for another 30 min at 37ºC. After exposure to 0.1 M sodium tetraborate decahydrate (pH 8.5) for 2 min at 37ºC, the cells were stained with fluorescein isothiocyanate–labeled antibodies to BrdU and PI for 30 min at 37ºC and were then analyzed with a FACSCanto II flow cytometer (BD Biosciences).

Immunofluorescence Staining of Neuro2a Cells

Neuro2a cells grown on glass coverslips were fixed in 1% paraformaldehyde for 10 min, washed with PBS, and permeabilized for 10 min with PBS containing 0.5% Triton X-100. They were then exposed to 5% nonfat milk in PBS before incubation with primary antibodies for 16 h at 4°C. After three washes with PBS-T, the cells were incubated with AlexaFluor-conjugated secondary antibodies for 45 min at room temperature, washed with PBS-T, exposed to DAPI (5 μg/ml) for 1 min, and then examined with an LSM780 confocal microscope (Zeiss).

Neurosphere Formation

Neurosphere was generated by the protocol of Larysa H. Pevny laboratory (Hutton and Pevny, 2008). Periventricular tissues of the 2-month-old adult brain were taken out, cut into smaller pieces, and incubated with 20 ml of enzyme solution [98 mM Na_2SO_4, 30 mM K_2SO_4, 5.8 mM $MgCl_2$, 0.25 mM $CaCl_2$, 1 mM HEPES-NaOH (pH 7.4), 20 mM Glucose, 0.001% Phenol Red, 2 mM Cysteine and 60 U Papain] for 40 min at 37°C. After removal of enzyme solution, samples were then sequentially incubated with 9 ml of light inhibitory solution [98 mM Na_2SO_4, 30 mM K_2SO_4, 5.8 mM $MgCl_2$, 0.25 mM $CaCl_2$, 1 mM HEPES-NaOH (pH 7.4), 20 mM Glucose, 0.001% Phenol Red, 0.1% BSA and 0.1% trypsin inhibitor] for 4 min at 37°C, 6 ml of heavy inhibitory solution [98 mM

Na_2SO_4, 30 mM K_2SO_4, 5.8 mM $MgCl_2$, 0.25 mM $CaCl_2$, 1 mM HEPES-NaOH (pH 7.4), 20 mM Glucose, 0.001% Phenol Red, 1% BSA and 1% trypsin inhibitor] for 2 min at 37°C, 5 ml of NEP basal medium (Neurobasal medium with B-27 and N-2) for 2 min at room temperature, and 2 ml of NEP complete medium (NEP basal medium with 100 ng/ml EGF and 10 ng/ml bFGF) at room temperature. Cells were then seeded in 1 well (9.5 cm^2) of ultra-low attachment 6-well plate (Corning) and were cultured under 5% CO_2 at 37°C. Neurosphere formed was counted using a hemacytometer at day 10.

Polysome Analysis

Neuro2a cells (1×10^7) were harvested, and cell extracts were layered onto linear sucrose density gradients [10–50% sucrose in 20 mM HEPES-NaOH (pH 7.6), 100 mM KCl, 5 mM $MgCl_2$, 1 mM dithiothreitol, and cycloheximide (100 μg/ml)] that had been prepared in open-top polyclear tubes (Seton) with the use of a Gradient Master. Samples were centrifuged at 131,000 × *g* for 3 h at 4°C in a P28S rotor (Hitachi Koki). Gradients were then fractionated (Towa). Polysome profiles were generated by continuous measurement of absorbance at 254 nm with a single-path UV-1 optical unit (AC-5200, ATTO) connected to a chart recorder (ATTO). Fractions of equal volume were collected and processed for RT-qPCR analysis.

Antibody

Anti-SETD5 (ab204363), anti-BrdU (ab6326), anti-Ki67 (ab15580), anti-H3K9me3 (ab8898), anti-H3K36me3 (ab9050), and anti-histone H3 (acetyl K9+K14+K18+K23+K27) (ab47915) antibodies were purchased from Abcam. Anti-DDB1 (5428), anti-HDAC3 (3949) and anti-PAF1 (12883) antibodies were from Cell Signaling Technology. Anti-SOX2 (sc-17320), anti-UBF (sc-13125), anti-RPA194 (sc-48385), anti-Cyclin D1 (sc-450), anti-Cyclin E1 (sc-481), and anti-Cyclin E2 (sc-28351) were from Santa Cruz Biotechnology. Anti-FLAG (F1804) and anti-Tubulin (T6074) were from Sigma-Aldrich. Anti-HA (11867423001) was from Roche. Anti-H4K16ac (07-329), anti-histone H4 (acetyl K5+K8+K12) (04-557), and anti-puromycin (MABE343) antibodies were from Millipore. Anti-TIP5 (100-401-v86) antibody was from Rockland. FITC-conjugated anti-BrdU (364103) was from Becton Dickinson. Alexa-555 conjugated anti-Rat IgG (A-21434) was from Thermo Fisher Scientific. HRP-conjugated anti-mouse IgG (W4021) and HRP-conjugated anti-rabbit IgG (W4011) were from Promega.

Statistical Analysis

Data are presented as means ± SEM and were analyzed by Student's t test, the paired t test, one-way ANOVA with or without Tukey's post hoc test, two-way ANOVA, or two-way repeated-measures ANOVA as indicated. A p value of <0.05 was considered statistically significant.

Data and Software Availability

Raw FASTQ files of RNA-seq data obtained in this study have been deposited in the DRA database (DRA009877).

SUPPLEMENTAL REFERENCES

Bradley, A., Anastassiadis, K., Ayadi, A., Battey, J.F., Bell, C., Birling, M.C., Bottomley, J., Brown, S.D., Burger, A., Bult, C.J., et al. (2012). The mammalian gene function resource: the International Knockout Mouse Consortium. Mamm. Genome *23*, 580–586.

Hutton, S.R., and Pevny, L.H. (2008). Isolation, culture, and differentiation of progenitor cells from the central nervous system. CSH Protoc. *2008*, pdb prot5077.

Mi, H., Muruganujan, A., and Thomas, P.D. (2013). PANTHER in 2013: modeling the evolution of gene function, and other gene attributes, in the context of phylogenetic trees. Nucleic Acids Res. *41*, D377–D386.

Murano, K., Okuwaki, M., Momose, F., Kumakura, M., Ueshima, S., Newbold, R.F., and Nagata, K. (2014). Reconstitution of human rRNA gene transcription in mouse cells by a complete SL1 complex. J. Cell Sci. *127*, 3309–3319.

Nakagawa, T., Hosogane, M., Nakagawa, M., Morohoshi, A., Funayama, R., and Nakayama, K. (2018). Transforming growth factor beta-induced proliferative arrest mediated by TRIM26-dependent TAF7 degradation and its antagonism by MYC. Mol. Cell. Biol. *38*, e00449-17.

Nakagawa, T., Lv, L., Nakagawa, M., Yu, Y., Yu, C., D'Alessio, A.C., Nakayama, K., Fan, H.Y., Chen, X., and Xiong, Y. (2015). CRL4(VprBP) E3 ligase promotes monoubiquitylation and chromatin binding of TET dioxygenases. Mol. Cell *57*, 247–260.

Pettitt, S.J., Liang, Q., Rairdan, X.Y., Moran, J.L., Prosser, H.M., Beier, D.R., Lloyd, K.C., Bradley, A., and Skarnes, W.C. (2009). Agouti C57BL/6N embryonic stem cells for mouse genetic resources. Nat. Methods *6*, 493–495.

Ran, F.A., Hsu, P.D., Wright, J., Agarwala, V., Scott, D.A., and Zhang, F. (2013). Genome engineering using the CRISPR-Cas9 system. Nat. Protoc. *8*, 2281–2308.

Santoro, R., Li, J., and Grummt, I. (2002). The nucleolar remodeling complex NoRC mediates heterochromatin formation and silencing of ribosomal gene transcription. Nat. Genet. *32*, 393–396.

Shin, K.J., Wall, E.A., Zavzavadjian, J.R., Santat, L.A., Liu, J., Hwang, J.I., Rebres, R., Roach, T., Seaman, W., Simon, M.I., et al. (2006). A single lentiviral vector

platform for microRNA-based conditional RNA interference and coordinated transgene expression. Proc. Natl. Acad. Sci. USA *103*, 13759–13764.

Skarnes, W.C., Rosen, B., West, A.P., Koutsourakis, M., Bushell, W., Iyer, V., Mujica, A.O., Thomas, M., Harrow, J., Cox, T., et al. (2011). A conditional knockout resource for the genome-wide study of mouse gene function. Nature *474*, 337–342.

Trapnell, C., Hendrickson, D.G., Sauvageau, M., Goff, L., Rinn, J.L., and Pachter, L. (2013). Differential analysis of gene regulation at transcript resolution with RNA-seq. Nat. Biotechnol. *31*, 46–53.

Trapnell, C., Pachter, L., and Salzberg, S.L. (2009). TopHat: discovering splice junctions with RNA-Seq. Bioinformatics *25*, 1105–1111.

White, J.K., Gerdin, A.K., Karp, N.A., Ryder, E., Buljan, M., Bussell, J.N., Salisbury, J., Clare, S., Ingham, N.J., Podrini, C., et al. (2013). Genome-wide generation and systematic phenotyping of knockout mice reveals new roles for many genes. Cell *154*, 452–464.